Pertti Myllys

Luminescence properties of GaN based diffusion injected light emitting diode structures

School of Electrical Engineering

Thesis submitted for examination for the degree of Master of Science in Technology.

Espoo 13.5.2015

Thesis supervisor:

Prof. Markku Sopanen

Thesis advisor:

M.Sc. (Tech.) Lauri Riuttanen

Aalto University
School of Electrical
Engineering

AALTO UNIVERSITY
SCHOOL OF ELECTRICAL ENGINEERING

ABSTRACT OF THE
MASTER'S THESIS

Author: Pertti Myllys

Title: Luminescence properties of GaN based diffusion injected light emitting diode structures

Date: 13.5.2015 Language: English Number of pages: 7+53

Department of Micro- and Nanosciences

Professorship: Optoelectronics Code: S-104

Supervisor: Prof. Markku Sopanen

Advisor: M.Sc. (Tech.) Lauri Riuttanen

Novel light emitting diode (LED) structures based on nanowires and surface plasmons have received an increasing amount of interest due to their potential to improve the performance. However, these novel structures based on conventional LED design model face challenges in efficient charge injection. An alternative current injection structure, called diffusion injected LED (DILED), was fabricated. The proposed structure can excite the active region located outside the p-n junction by bipolar diffusion, thus providing a possible solution to most of the challenges encountered.

In this thesis, the focus is on the luminescence properties of three different types of GaN based DILED structures, *i.e.*, two buried MQW DILED and a surface quantum well (QW) DILED structures. The goal is to characterize and to determine the effectiveness of these novel devices. The studied structures were measured by electroluminescence (EL) including temperature controlled situation, photoluminescence (PL) and by micro-photoluminescence (μ-PL).

In contrast to the conventional LEDs, the emission of DILED structures increased with increasing temperature. The figure of merit values, such as external quantum efficiency (EQE), optical output power and wall-plug efficiency, were relatively low with all buried DILED structures. However, all these values increased with increasing injection current, which is in contrast to conventional GaN based LEDs. The emission of surface QW DILED structures was too weak to measure with optical fiber, so only PL and μ-PL measurements were carried out. All the DILED structures operate by an alternative current injection method, which provides a new possibility for device design and help to overcome some of the challenges when developing GaN based LEDs.

Keywords: III-nitrides, carrier injection, charge carrier diffusion, DILED, GaN, LED, MOVPE

AALTO-YLIOPISTO
SÄHKÖTEKNIIKAN KORKEAKOULU

DIPLOMITYÖN
TIIVISTELMÄ

Tekijä: Pertti Myllys

Työn nimi: GaN-pohjaisten diffuusioinjektoitujen hohtodiodirakenteiden luminesenssi ominaisuudet

Päivämäärä: 13.5.2015 Kieli: Englanti Sivumäärä: 7+53

Mikro- ja nanotekniikan laitos

Professuuri: Optoelektroniikka Koodi: S-104

Työn valvoja: Prof. Markku Sopanen

Työn ohjaaja: DI Lauri Riuttanen

Uusiin nanorakenteisiin perustuvien hohtodiodien (LED, light emitting diode) odotetaan parantavan LED:en suorituskykyä, mutta perinteiseen LED-malliin perustuvat uudet rakenteet kohtaavat kuitenkin haasteita sekä valmistuksessa että varaustenkuljettajien syötön hyötysuhteessa. Näiden ongelmien ratkaisemiseksi on uudenlainen virransyöttörakenne valmistettu perustuen varauksenkuljettajien diffuusioon. Diffuusioinjektoiduissa LED-rakenteissa (DILED, diffusion injected light emitting diode) aktiivinen alue sijaitsee pn-liitoksen ulkopuolella ja varauksenkuljettajat diffusoituvat aktiiviselle alueelle samalta puolelta.

Tässä diplomityössä keskitytään kolmen erilaisen GaN-pohjaisen DILED-rakenteen luminesenssi ominaisuuksiin. Rakenteet sisältävät kaksi erilaista haudattua monikvanttikaivorakennetta ja yhden pintakvanttikaivorakenteen. Tavoitteena on karakterisoida ja selvittää kyseisten uusien laitteiden tehokkuus ja soveltuvuus uutena LED-mallina. Rakenteet mitattiin elektroluminesenssi (EL), mukaan lukien lämpötilakontrolloitu tilanne, fotoluminesenssi (PL) sekä mikrofotoluminesenssi (μ-PL) menetelmillä.

Toisin kuin perinteiset LED:t, DILED-rakenteiden emissio kasvaa lämpötilan kasvaessa. Hyvyysluvut, kuten ulkoinen kvanttihyötysuhde, optinen lähtöteho ja tehohyötysuhde, olivat suhteellisen alhaiset jokaisessa haudatussa monikvanttikaivorakenteessa. Jokaisen hyvyysluvun arvo kuitenkin kasvoi syötetyn virran suhteen, mikä on perinteisille GaN-pohjaisille LED-rakenteille päinvastainen. Pintakvanttikaivollisten DILED:en emissio oli liian heikko mitattavaksi optisella kuidulla, joten vain PL ja μ-PL mittaukset suoritettiin. Kaikki DILED-rakenteet tarjoavat vaihtoehtoisen tavan virran syötölle, uuden mahdollisuuden laitesuunnittelulle sekä auttavat ratkaisemaan GaN-pohjaisten LED:en kehityksessä ilmeneviä haasteita.

Avainsanat: III-nitridi, varauksen syöttö, varauksenkuljettaja diffuusio, DILED, GaN, LED, MOVPE

Preface

This thesis was carried out in the Department of Micro- and Nanosciences at Aalto University School of Science and Technology.

First, I would like to thank Professor Markku Sopanen for giving me a chance to be part of the research team to complete my thesis and D.Sc. (Tech.) Sami Suihkonen for providing me with such an interesting research topic. Second, a big thanks goes to my instructor Lauri Riuttanen for his excellent guidance during this thesis. In addition, I would like to express my gratitude to Ville Pale for his expertise using the SNOM-tool used in the μ-PL measurements. Finally, I would thank my family for supporting me through my education.

Otaniemi, 10.5.2015

Pertti J. Myllys

Contents

Symbols and abbreviations

Symbols

c	speed of light
E	Energy level
E_c	Conduction band
E_F	Fermi level
E_g	Band gap
E_v	Valence band
h	Planck's constant
$\mathbf{k}$	Wave vector
k_B	Boltzmann constant
n	Electron concentration
n_i	Intrinsic carrier density
p	Hole concentration
T	Temperature
η	Wall-plug efficiency
λ	Wavelength

Abbreviations

III-N	III-nitride
AlGaN	Aluminum Gallium Nitride
BCC	Body-Centered Cubic
CO_2	Carbon Dioxide
CSL	Current Spreading Layer
Cp_2Mg	Bis(cyclopentadienyl)magnesium
DHJ	Double Heterojunction
DILED	Diffusion Injected Light Emitting Diode
EBL	Electron Blocking Layer
EL	Electroluminescence
EQE	External Quantum Efficiency
FCC	Face-Centered Cubic
GaN	Gallium Nitride
HCP	Hexagonal Close-Packed
HEMT	High-Electron-Mobility Transistor
HVPE	Hybride Vapor Phase Epitaxy
I-V	Current-Voltage
ICP-RIE	Inductively Coupled Plasma-Reactive Ion Etching
InGaN	Indium Gallium Nitride
IQE	Internal Quantum Efficiency
ITO	Indium Tin Oxide
LED	Light Emitting Diode
μ-PL	Micro-Photoluminescence
MBE	Molecular Beam Epitaxy
MOCVD	Metalorganic Chemical Vapor Deposition
MOVPE	Metalorganic Vapor Phase Epitaxy
MQW	Multi-Quantum Well
PL	Photoluminescence
QCSE	Quantum-Confined Stark Effect
QW	Quantum Well
SC	Simple Cubic
SiC	Silicon Carbide
SL	Superlattice
SNOM	Scanning Near-Field Optical Microscope
TMAl	Trimethyl Aluminum
TMGa	Trimethyl Gallium
TMIn	Trimethyl Indium
YL	Yellow Luminescence

1 Introduction

Nowadays the efficient use of energy plays an important role in global consumption of electricity, as well as in the global dependence on fossil fuels. Renewable energies, such as solar, wind, hydro- or bioenergy, are becoming feasible due to long-term commitments in order to reduce carbon dioxide (CO_2) emissions globally. In 2005, power grid based lighting consumed approximately one fifth of the total electricity produced worldwide [1, 2]. The consumption of electricity in households will increase due to the increasing number of electrical devices. This consumption can be reduced when new energy-saving technologies will be adopted, *e.g.*, in lighting as well as in consumer electronics. Saving energy would also decrease the CO_2 emission significantly.

Promising solutions for low-carbon energy production and efficient energy use are optoelectronics and photonics. One potential application is light emitting diode (LED) structure, that is already being adopted in lighting applications throughout the globe. The number of LED structures has increased in our everyday life in the past decades. LEDs can be found in TVs, mobile phones, displays, as light sources, traffic lights, advertising panels, in communication fibers etc. The numbers of applications are vast. The advantages compared to traditional light sources include that LEDs are energy efficient, *i.e.*, the power consumption is low, they produce less heat than conventional light bulbs and have longer lifetime [2].

LEDs may produce light in the ultraviolet, visible and infrared parts of the spectrum. They have become a potential alternative to incandescent lamps, which are soon to be banned because of their energy inefficiency, but also to fluorescent lamps and tubes with the decrease of LEDs manufacturing costs [2]. However, one of the most challenging colors for LED to produce was blue. The reason for this was the fact that the material, from which the blue LED was fabricated, *i.e.*, gallium nitride (GaN), was difficult to fabricate as a high-efficient LED device because of the challenges to p-dope GaN. Because of this, there have also been problems to produce, *e.g.*, full-color displays, which need the three primary colors. In addition, this combination is also needed to produce white LED devices. Since the 1970s, elements such as Zn, Cd, Be and other similar group II elements has been tried for doping p-type GaN. However, without desired results. [3] Nowadays p-type doping for GaN is typically achieved using Mg.

GaN based LEDs are predominantly used in today's LED lamps by emitting blue light, which is converted to white light using yellow phosphors. The fast progress in p-type doping, material quality, InGaN multi-quantum well (MQW) structures and light extraction have made III-nitrides (III-N) LEDs the driving force of solid-state lighting. The best commercial LEDs efficiencies may reach up to 84 % at normal operating conditions [4]. Even though the LEDs are said to be highly efficient, are there still much to improve. One of the most important bottlenecks in the development of high-efficiency LEDs is the so-called efficiency droop [5], *i.e.*, the

decrease of the LED efficiency when the input power increases. A desired result is to reduce the amount of the efficiency droop, thus increasing the efficiency and optical output power of LEDs, which is why structures, *e.g.*, based on nanowires and surface plasmons have received an increasing amount of attention. Such nanostructured LED devices have the possibility to increase the efficiency, such as internal quantum efficiency (IQE) with low efficiency droop, as well as provide more freedom in structure engineering [6, 7]. However, there are some practical challenges for these devices as well, including difficult fabricating process and efficient current injection to the active region close to the surface. Riuttanen *et al.* [8] has demonstrated an alternative charge injection method based on carrier transport by bipolar diffusion. They fabricated two buried MQW III-N diffusion injected LED (DILED) structures and a surface QW DILED structure, which all represents a new device design where the active region is located outside the p-n junction. This is in contrast to the conventional LED model, where the active region is sandwiched between the p- and n-layers. The fabricated structures introduces a possible solution to help overcome the challenges encountered in fabrication and the current injection with nanowire and surface plasmon based LEDs.

In this thesis, the focus is on the luminescence properties of three different types of GaN based DILED structures. The active region of the two of them were buried under the p-n junction. In these buried structures a MQW stack was used as an active region. The third structure had a single QW as an active region on top of the p-n junction. Different layouts of those fabricated DILED structures are characterized. Also, a conventional GaN based LED structure is briefly analyzed as a reference LED in which the DILED structures are compared to. The buried MQW DILED, as well as surface QW DILED, structures were measured by electroluminescence (EL), including temperature controlled situation where a Peltier element was used to maintain the desired temperature, by photoluminescence (PL) and micro-photoluminescence (μ-PL).

Introduction to the theories behind semiconductors are briefly presented in Chapter 2 including crystal structures, band gaps, p-n junctions and QWs. In Chapter 3 is the basic principle of LED presented, including background information about GaN, and the studied DILED structures. This is followed by the experimental section in Chapter 4 where the fabrication processes of DILED structures, all the used equipments and measurement methods are described. In Chapter 5 are the measurement results presented and discussed and finally the conclusion in Chapter 6.

2 Basics of Semiconductors

2.1 Crystal Structure

The atoms in a crystalline material are arranged in a three-dimensional periodic fashion, which is described by a repeating pattern of mathematical points that extends throughout space of the crystal called a lattice. The simplest repeating unit in a crystal is called a unit cell that is representative of the entire lattice. Generally there are 14 types of crystal lattices, of which the most common are the simple cubic (SC) lattice, the body-centered cubic (BCC) lattice, the face-centered cubic (FCC) lattice and the hexagonal closest-packed (HCP) lattice. [9]

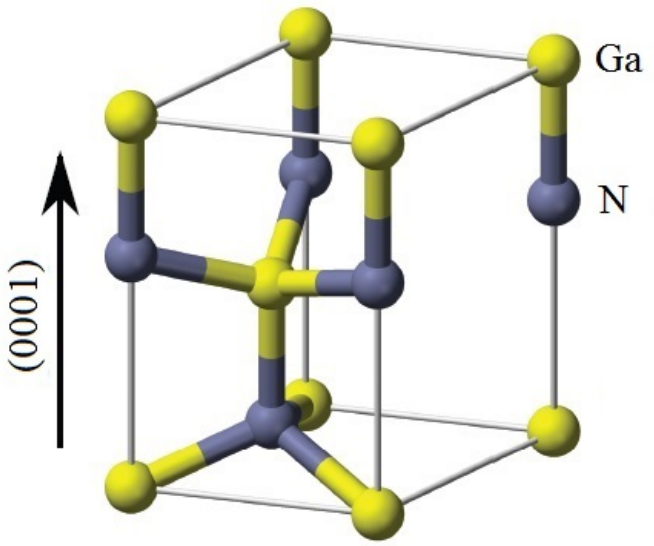

Figure 1: Illustration of hexagonal wurtzite structure of GaN in (0001) crystal orientation. Gray spheres represent N atoms and yellow Ga atoms. [10]

Many important semiconductors have so-called diamond, zincblende or wurtzite lattice structures. Each belong to tetrahedral phases in which each atom is surrounded by four equidistant nearest neighbors which lie at the corners of a tetrahedron. In the case of III-N, the group can crystallize either in hexagonal wurtzite or zincblende structure, which both can be grown by epitaxial thin film methods and are widely studied [11]. The wurtzite lattice can be considered as two interpenetrating HCP lattices. A typical illustration of a hexagonal wurtzite structure in (0001) crystal orientation is shown in Figure 1. In this case the grey spheres represent N atoms and yellow Ga atoms.

2.2 Electronic Band Structure

In an isolated atom, the electrons can have certain discrete energy levels. When two identical atoms are brought close to each other, the energy levels will split into two levels by the interaction between the atoms. This is due to the Pauli exclusion principle which states that no two electrons can occupy the same quantum mechanical state in a given system [9]. If a large number of isolated atoms are brought together to form a solid, the outer electrons of different atoms interact and overlap with each other due to the attraction and repulsion forces, thus splitting and shifting the energy levels until so-called energy bands are formed. In semiconductors, when temperature $T = 0$ K, the electrons occupy the lowest energy levels filling all available energy states. This band is called the valence band, while the upper band, called the conduction band, will be completely empty. Between these adjacent energy bands are forbidden regions called band gaps, E_g, where there are no allowed energy levels. The band gap is the smallest energy difference between the valence and the conduction band, which is required to free an electron from the valence band up to the conduction band. If the band gap between the valence and conduction band occurs between the same **k**-space values, the semiconductor is called a direct band gap material, while with different **k**-values it is called an indirect band gap material [12].

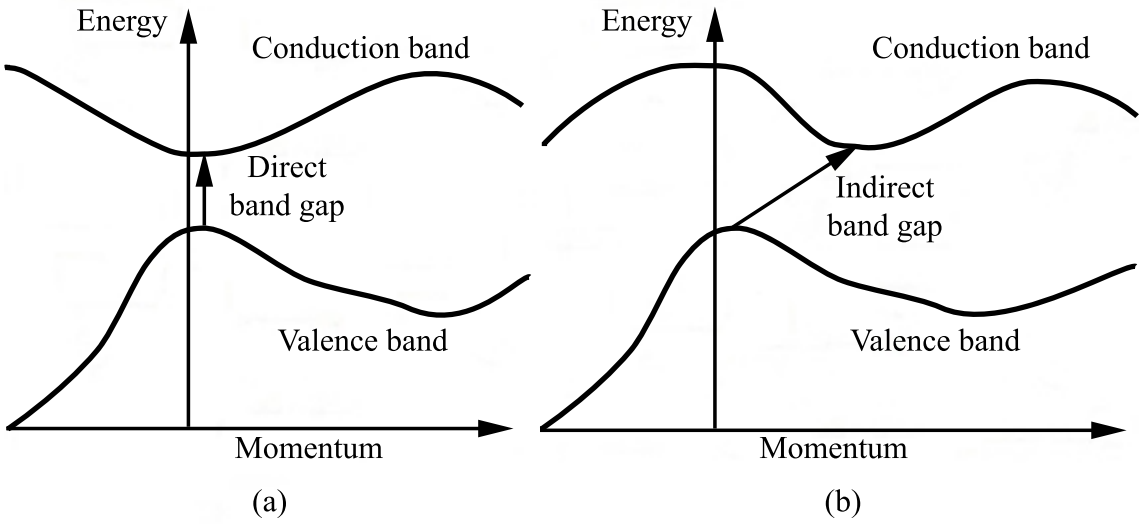

Figure 2: Energy band structures for (a) direct band gap, and (b) indirect band gap semiconductors. For optoelectronic devices the direct band gap is preferred because the emission of a photon is more likely to occur with direct band gap than with indirect band gap.

An electron transition from valence to conduction band does not need a change in momentum in a direct band gap material. However, a change in momentum is required, *e.g.*, via interaction with a phonon, in the case of indirect band gap. Also, a direct band gap material is more likely to emit a photon than indirect band gap

material. Therefore, the indirect transition process is much more unlikely to happen than the direct transition. A representation of direct and indirect band gap material semiconductors are shown in Figure 2. In the case of optoelectronic devices the direct band gap of III-V semiconductors are the most important [13].

The nature of the energy bands determines the type of a material, *i.e.*, is it a conductor, a semiconductor, or an electrical insulator. The conduction band in conductors is either partially filled or overlaps the valence band, so there is no band gap like in semiconductors and insulators. Also, conductors have very low value of resistivity. Electrons are free to move with small applied electric field because there are plenty of unoccupied states.

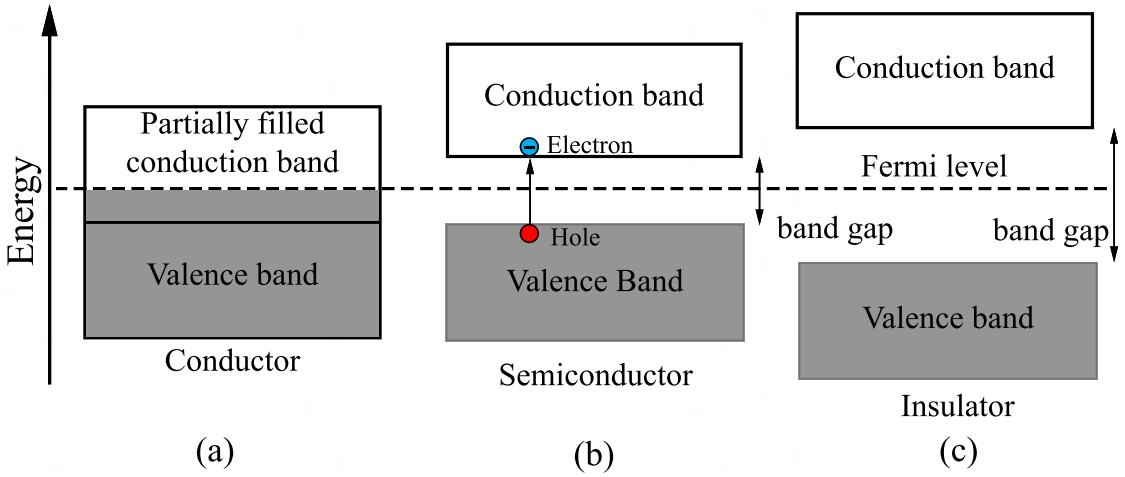

Figure 3: Schematic representation of energy bands for (a) a conductor with partially filled conduction band, (b) a semiconductor, and (c) an insulator with corresponding Fermi level.

In an insulator the valence electrons form strong bonds between neighboring atoms. At absolute zero temperature, the highest band that is completely filled is the valence band. There are no free electrons to participate in current conduction. Electrons occupy all energy levels in the valence band while all the corresponding levels in the conduction band are empty. Thermal or applied energy by the electric field excites only few electrons from the valence band to the conduction band.

The conduction band of a semiconductor consists of many allowed, empty energy levels. At absolute zero temperature, a semiconductor has an empty conduction band and full valence band making it an insulator. The electric conductivity increases as some states in the conduction band are filled by thermal excitation. However, in order to know how many electrons will fill these levels, one must first consider how many energy levels there are within a given range of energy and how likely each level is occupied by an electron. A probability function called the Fermi-Dirac distribution determines what the probability of an energy level, E, will be when occupied by an

electron and is expressed by

$$f(E) = \frac{1}{1 + e^{(E-E_F)/(k_B T)}} \tag{1}$$

where E_F is the energy of Fermi level, k_B is the Boltzmann constant and T is the absolute temperature. [14] The Fermi level is the energy at which the probability of occupancy by an electron is exactly 50 %. In Figure 3, the energy bands of conductors, semiconductors and insulators with corresponding Fermi levels are presented. More detailed information can be found in Ref. 14.

2.3 Semiconductors

Semiconductors have affected the world and our everyday life with great impact and they play an important role in applications nowadays. Their importance arises from the fact that their electrical properties are extremely sensitive to very small concentration of impurities [9], but also from the ability to act as conductors and insulators. It has been said that the earliest systematic study of semiconductor devices is attributed to Braun in 1874 with a metal-semiconductor contact [14]. He was the first to discover that the resistance of contacts between metals and metal sulfides depended on the magnitude and polarity of the applied voltage. When an electron is removed from a valence band, it leaves a vacancy behind. This vacancy can be occupied with an electron from the neighboring atom which in turn leaves another vacancy behind and so on. In this way the vacancy can travel through the material and serve as an additional current carrier. Thus, the vacancy is treated as a positive charge carrier in semiconductors moving in the opposite direction to that of an electron and is called a hole.

The conductivity of a pure semiconductor can easily be modified by introducing impurity elements, *i.e.*, dopants, into the crystal. There are two basic classifications to define semiconductor types. When a semiconductor is doped, it is called an extrinsic semiconductor while the undoped is called an intrinsic semiconductor. Extrinsic semiconductors have a small amount of impurity, which modifies the electrical properties of the semiconductor and improves its conductivity, forming either n- or p-type semiconductor. In n-type semiconductor the impurity atom donates excess electrons, which are free to act as majority charge carriers. Such atoms are known as donors. In p-type semiconductor there is a shortage of electrons. The impurity atoms, known as acceptors, generate holes ready to accept electrons. In such a semiconductor there are an excess of holes free to act as majority charge carriers. An intrinsic semiconductor is a pure material which possesses poor conductivity, because the valence band holes and conduction band electrons are present in equal numbers. When an intrinsic semiconductor is in equilibrium, the concentration of electrons in the conduction band, n, and the concentration of holes in the valence band, p, are equal, *i.e.*, $n = p = n_i$, where n_i is the intrinsic carrier density. [11]

In solid-state electronics the so-called p-n junctions are of great importance in understanding semiconductor devices. The essential principle is that the conductivity of the material is controlled by impurity concentrations from one region to another which allow the current to flow within the materials. A p-n junction is formed from a semiconductor crystal which one side is doped with p-type impurities and the other side with n-type impurities. A p-type semiconductor contains a large concentration of holes with few electrons, while the n-type has more electrons than holes. There are four different currents across the p-n junction, the diffusion current and drift current for both holes and electrons. When a p-n junction is formed, a large carrier concentration gradient at the junction cause carrier diffusion. Electrons in the n-region diffuse into the p-side leaving positive donors in the n-type region, while holes in the p-region diffuse into the n-side leaving negative acceptors in the p-type region, thus creating a depletion zone [13, 14]. This zone creates an electric field that is in the opposite direction to the diffusion current for each charge carrier. At thermal equilibrium without external forces, the electron and hole current across the junctions cancel each other. This means that the drift current due to the electric field equals to the diffusion current and cancels this.

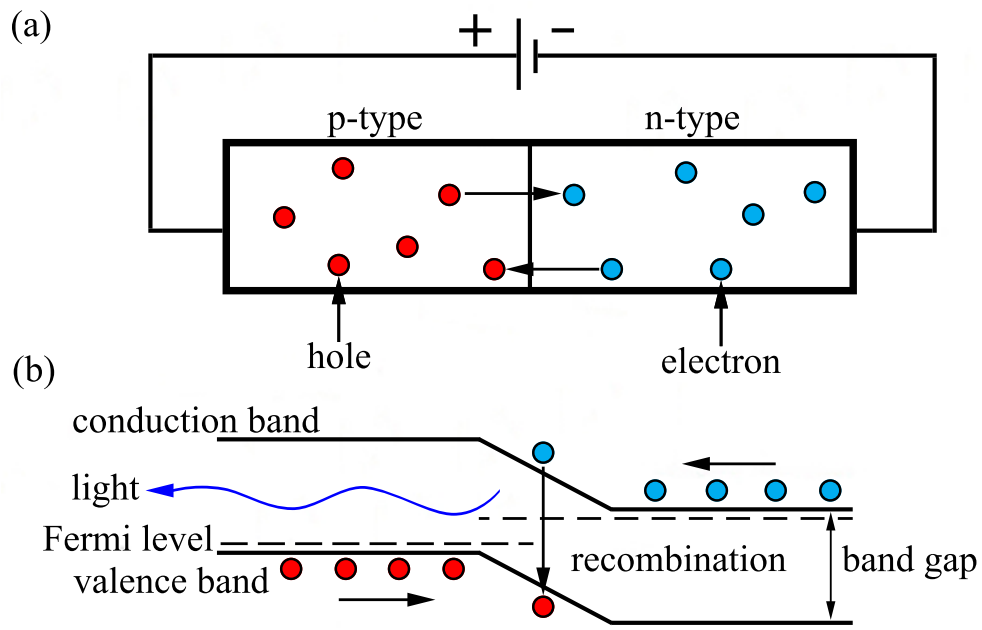

Figure 4: Schematic illustration of a p-n junction (a) structure and (b) energy bands including Fermi levels under forward bias. The light emitted is due to the recombination effect of electrons and holes.

If a potential difference is applied to the p-n junction, with p-side being in higher potential, the semiconductor is said to be forward biased. The applied voltage reduces the electrostatic potential across the depletion region and the free electrons in the n-type region, and holes in the p-type region, flow toward the junction where they recombine. Current flows continuously as electrons are moved to the lower potential

side while holes are moved to the higher potential side. Should the n-type be at higher potential, both holes and electrons will move away from the junction and the semiconductor is reverse biased without current flow. Figure 4 shows an illustration of a forward biased p-n junction (a) structure and (b) corresponding energy bands including Fermi levels with electrons, blue circles, at the n-side and holes, red circles, at p-side. Light is emitted through the recombination process of electrons and holes. Under forward bias the Fermi level is altered by the amount of applied positive voltage.

2.4 Quantum Wells

Quantum wells (QWs) are thin layers of semiconducting material and their properties are derived from the quantum confinement of charge carriers, *i.e.*, electrons and holes. A QW is typically formed by three layers of materials, such that the middle layer has the lowest band gap energy, *e.g.*, by introducing indium into GaN. Both electrons and holes see this lower energy layer as a "well". Therefore a QW confines carriers into two dimensional system. Typical growth methods for QW structures are molecular beam epitaxy (MBE) and metalorganic chemical vapor deposition (MOCVD), also known as metalorganic vapor phase epitaxy (MOVPE). MOVPE technique is described in detail in Section 4.1.

The basic properties of QWs can be understood through a simplification in one-dimension called the infinite well model, in which a particle is confined between infinitely high, insurmountable potential energy walls. The physics behind the QW and the infinite well model is presented with Schrödinger equation for the studied particle. (Note that the detailed information about the Schrödinger equation or its solutions is out of scope of this thesis. For more detailed information, please refer to Ref. 13 or 15.) Because the particle can be approximated in one-dimension, the time-independent Schrödinger equation is reduced from three-dimensional into one-dimensional solution. Classically, the particle would bounce back and forth in the well, but in this quantum-mechanical solution of the Schrödinger equation it will be a standing wave. The solution for Schrödinger equation, where a wave function for a given potential energy is solved, is one remarkable observation obtained. It implies that the particle's energy is not arbitrary, but is quantized, meaning that the energy of a particle has certain discrete values. [15]

When there is no electric field in QWs, electron and hole wavefunctions are confined in the QW. But when an electric field is applied across the QW, the energy bands of QW will bend in the active region. It separates electrons and holes, thus reducing the overlap of their wavefunctions as well as the separation energy. This decreases the radiative recombination efficiency of electrons and holes and is called the quantum-confined Stark effect (QCSE). The strength of the QCSE depends on either due to the polarization-related electric fields that are induced by lattice mismatch of (InGaN) QW and (GaN) barrier [16] or on the externally applied voltage to the device [17]. Figure 5 shows an example of (a) a single InGaN/GaN QW

structure, (b) its energy levels and (c) how the QCSE affects the band diagram of QW under electric field with a band gap of E_{QW2}. E_c and E_v corresponds the energy of the conduction and valence band, respectively, n is a positive integer, E_g the energy of the band gap and E_{QW} the band gap energy of the QW. Because of the QCSE, is $E_{QW} > E_{QW2}$.

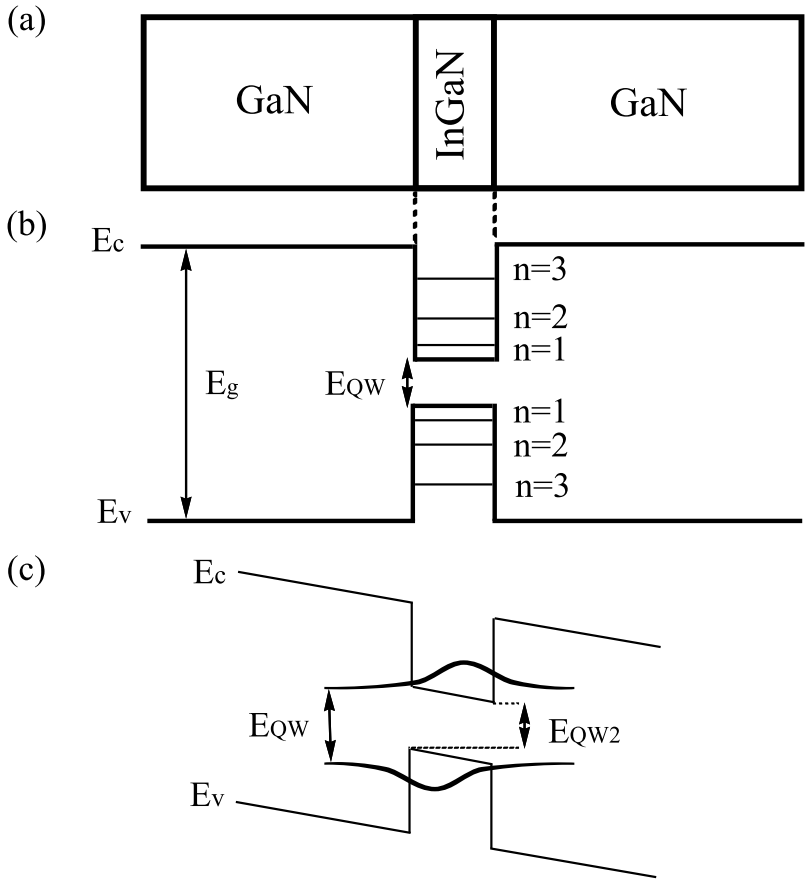

Figure 5: Illustration of a single InGaN/GaN QW (a) structure, (b) energy levels and (c) quantum-confined Stark effect with $E_{QW} > E_{QW2}$.

3 Light Emitting Diodes

In 1907 H. J. Round discovered electroluminescence phenomenon which was not well understood at that time. Nevertheless, Round reported his observations and that was a starting point for LED structures. [14, 18] However, the first LED patent was filled by O. V. Losev in 1929, but this discovery was quickly forgotten. Nick Holonyak in 1962 was the first to develop LED that emitted light in the visible part of the spectrum, namely a red LED. [2] LEDs play an important role as a versatile light source and as part of many applications because of their small size, efficiency, reliability and brightness. Also, they have the potential of converting electricity into light with near-unity efficiency [18].

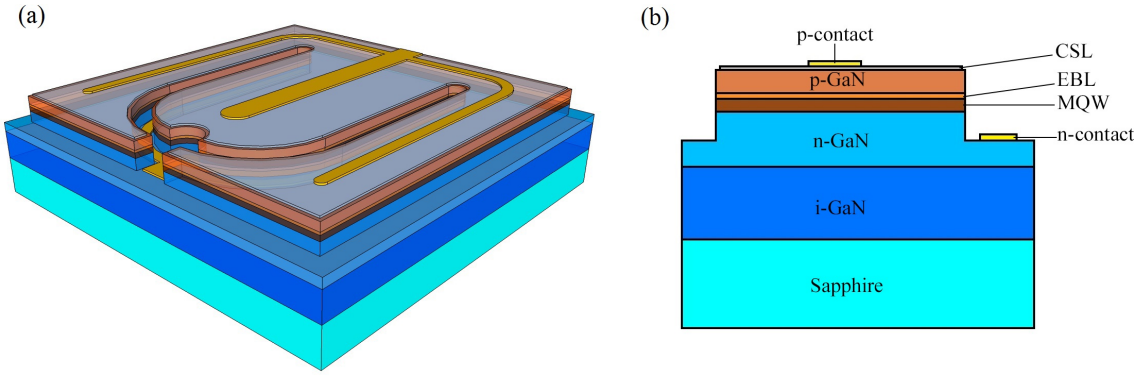

Figure 6: (a) Illustration and (b) a cross-sectional view of a conventional LED structure.

A forward biased p-n junction based LED is one of the simples optoelectronic devices in which the electrons (and holes) are injected into the p-side (and n-side). The injected minority charge carriers recombine with the majority charge in the depletion region. However, the efficiency of such LED is small, which is why nowadays LEDs are mainly based on QWs. In Figure 6 (a) is an illustration and (b) a cross-sectional view of a conventional LED structure presented with MQW, *i.e.*, active region, sandwiched between p- and n-GaN.

In QW based LEDs the carriers tend to escape from the active layer into the confinement layers. In order to reduce this carrier leakage, electron-blocking layers (EBL) are used. Such layers are regions with higher band gap energy, *e.g.*, aluminum gallium nitride (AlGaN), located between the active region and the p-type semiconductor layer. The EBL assists to prevent the electron leakage, but does not impede the hole flow into the active region when it is properly implemented. In addition, the efficiency of a LED can be improved by using a current spreading layer (CSL). It is a transparent layer, which is deposited on the top of the p-type semiconductor, *i.e.*, p-GaN in Figure 6, and under the top contact. CSLs are used to spread the current under the top electrode into regions, which are not covered by the electrode. Without the CSL, the emitted light would be generated in the vicinity of the electrode, which

would be inefficient with poor electric conductivity materials, *e.g.*, p-GaN, thus resulting in low extraction efficiency. [18] CSLs are typically fabricated from indium tin oxide (ITO) [19], but also a thin Ni/Au layer can be used.

In direct band gap semiconductors the radiative recombination lead to light emission. The emitted photon energy is approximately equal to the band gap energy and thus can be varied by using materials with different band gaps. The energy of an emitted photon can be expressed as

$$E_g = \frac{hc}{\lambda}, \tag{2}$$

where h is Planck's constant, c the speed of light and λ the wavelength of the emitted light. In Figure 7 (a) is a simplified illustration of the conventional LED structure and (b) its corresponding energy bands including an EBL. For simplicity, only one QW is presented instead of MQW. The electrons and holes (represented by blue and red circles, respectively, in Figure 7) recombine at the bottom of the QW, thus emitting light. By varying the position of the energy level in the QW, E_{QW}, the wavelength of the emitted light can be changed.

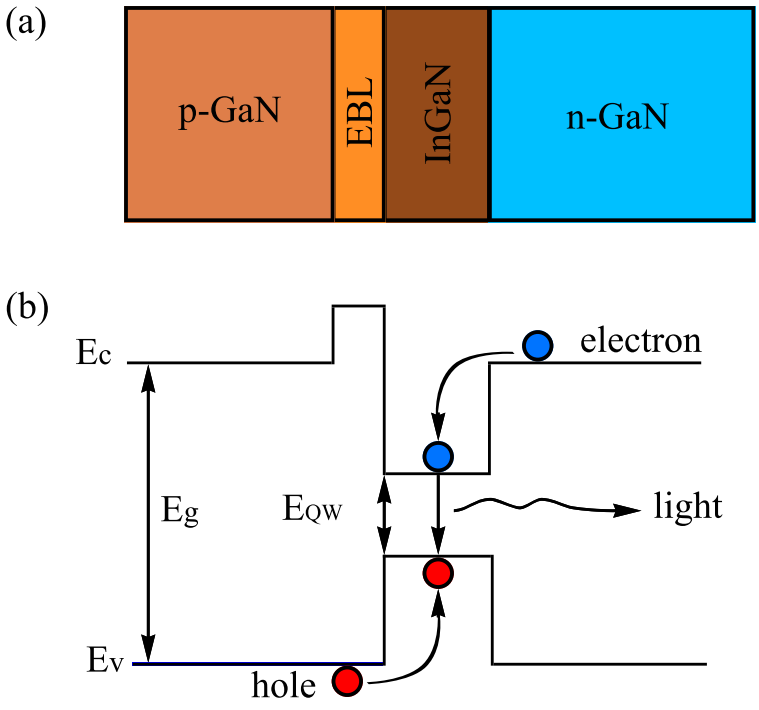

Figure 7: Illustration of (a) a simplified conventional LED structure and (b) its corresponding energy bands including an EBL. For simplicity, only one QW is presented instead of MQW.

In indirect gap semiconductors, the light emission efficiency is poor due to non-radiative recombination. The energy of an electron is converted to the vibrational

energy of lattice atoms, *i.e.*, phonons, converting the energy into heat rather than light, which in the case of LEDs is an unwanted process. The purpose of LEDs is to convert electrical energy into light in the ultraviolet, visible or infrared region of the spectrum. That in mind, what matters is the amount of emitted light from the device. The parameter to measure the efficiency of light emitted out from the LED device is called the external quantum efficiency (EQE) which can be defined as

$$EQE = \frac{number\ of\ photons\ emitted\ externally}{number\ of\ carriers\ passing\ junction} \tag{3}$$

EQE can be split into two parts, to the IQE and to the optical extraction efficiency. IQE is defined as the ratio of photons generated inside the QWs to the total number of electrons injected into the LED, and the optical extraction efficiency as the ratio of photons emitted from the LED to photons generated inside the LED QWs. Thus, the EQE would be IQE times optical extraction efficiency. EQE values for GaN based LEDs has increased considerably over the years from 0.18 % [20] up to 80 % [4].

3.1 Gallium Nitride

The group III-N compounds, *e.g.*, GaN, have become of great importance for a wide band gap semiconductor material as high speed, high power electronics and high temperature electronics, as well as LEDs and detectors. GaN, as well as its related compounds, can crystallize both in the zincblende and hexagonal wurtzite structure, from which the wurtzite structure is more common [21]. GaN is also a direct band gap material, which makes it highly favorable for optoelectronic devices.

Table 1: Properties of important III-N semiconductors at room temperature [2, 18, 22, 23, 24]

	AlN	**GaN**	**InN**
Crystal structure	Wurtzite	Wurtzite	Wurtzite
Band gap: direct (D)	D	D	D
Lattice constant at 300 K, (Å)	3.11	3.19	3.55
Energy band gap, (eV)	6.28	3.44	0.77

The two most common substrates for the epitaxial growth of GaN are c-plane (0001) sapphire and silicon carbide (SiC), which both have hexagonal lattice. Most of the commercial GaN based LEDs are grown on (0001) sapphire [2]. The currently used growth method of GaN is in the form of epitaxial layers typically by MOVPE. However, growing GaN onto a sapphire surface is somewhat problematic because of the lattice mismatch between these materials. The lattice parameters and the thermal expansion coefficients of sapphire, or SiC, are not well matched to those of GaN. This generates huge densities of dislocations in the structure, which in turn propagate to the surface deteriorating the performance of optical devices [25]. The lattice

parameter of sapphire in (0001) plane is 4.758 Å, whereas GaN has 3.189 Å [2, 21]. Without the lattice rotation, the lattice mismatch would be +50 %. However, if the GaN lattice is rotated by 30^o with respect to the sapphire lattice, the lattice mismatch is reduced to −13.8 % [2, 26]. Sapphire is very stable in its mechanical and chemical properties [18]. However, it is also a good electrical and thermal insulator causing current to crowd near the contacts and increase temperature, which both are problematic effects in GaN based LEDs [19].

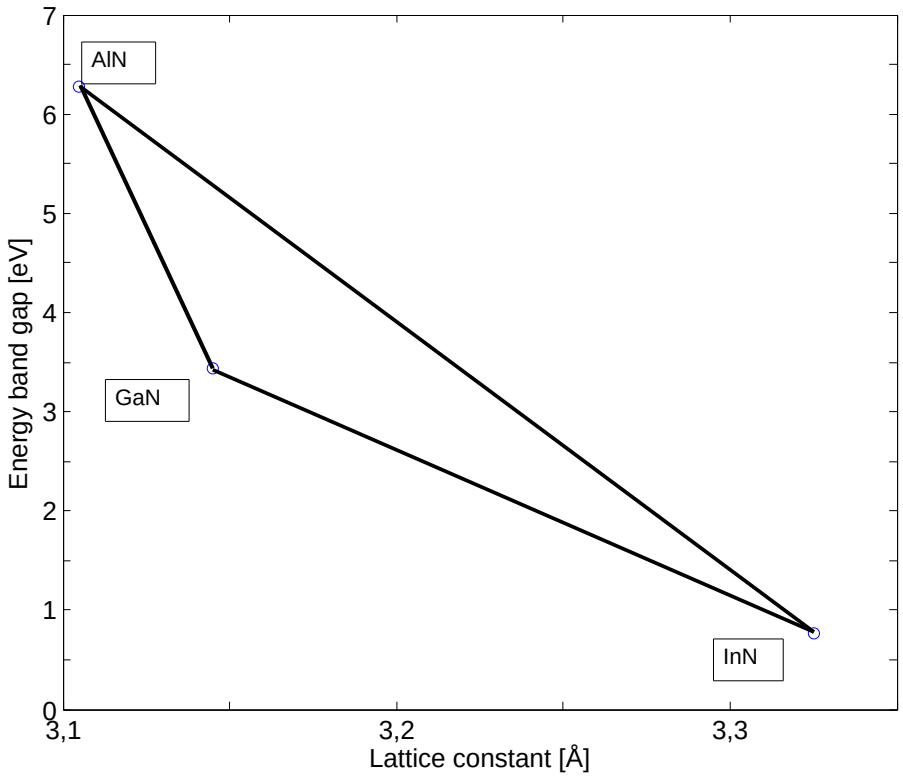

Figure 8: Band gap versus lattice constant of important III-N semiconductors according to the values in Table 1.

Table 1 presents the properties of important III-N semiconductor materials at room temperature. One should notice that, the values have been adapted from different references, *e.g.*, recent studies [2, 22, 23, 24] have presented InN energy band gap values from 0.7 to 0.8 eV, whereas in some older studies [3] the corresponding values are presented to be 1.9 eV. Figure 8 shows the band gap versus lattice constant demonstrated according to Table 1.

Development of GaN Based LEDs

GaN crystals have been grown using the hybride vapor phase epitaxy (HVPE) method, but the quality of the crystal was not easily achieved due to contamination until new growth techniques, such as MBE and MOVPE, were developed [21]. Amano

et al. noticed that by using AlN buffer layers the quality of GaN crystals could be improved considerably [26]. Later Nakamura S. obtained a high quality GaN film using a GaN buffer layer, which was clearly superior compared to the AlN buffer layer [27].

The III-N alloy appeared to be a promising solution for blue light emitting devices, because its band gap varies from 0.7 eV to 3.4 eV. A high quality InGaN film was succeeded to grow on GaN with promising results [28]. Last crucial step for producing efficient blue LEDs was the growth and doping of p-type alloys in order to produce p-n junctions. However, the major challenge in developing a blue LED was producing p-type GaN. Nakamura *et al.* found that after GaN crystal growth a low resistivity Mg-doped p-type GaN film could be obtained by thermal annealing [29]. Nowadays the thermal annealing is commonly used to obtain MOVPE grown p-type GaN layers [21].

There are still much to develop for high-efficiency LEDs. One major challenge hindering the development of GaN based LED is their efficiency droop, *i.e.*, the decrease of the efficiency from its peak value when the input power is increased. The efficiency droop has been studied actively [5] and the explanation of physical mechanism has been highly debated [30]. The mechanisms to explain efficiency droop include electron leakage due to polarization mismatch, defect related mechanisms, and Auger recombination [5, 31, 32], but none of these are generally accepted. So far the only accepted general conclusion is that the droop is triggered by the excess carrier density of the active region [33]. Because of the efficiency droop, the output power of GaN based LEDs is limited, thus making it a significant problem.

3.2 Diffusion Injected Light Emitting Diodes

Majority of inorganic LEDs are based on a double heterojunction (DHJ) structure. The current injection principle in these structures has remained essentially unchanged. In each of these structures is the current transport enabled by conventional configuration where the active region, *e.g.*, MQW stack, is sandwiched between p- and n-regions as was seen in Figure 6 (b). Novel III-N LED structures based on nanowires and surface plasmons are expected to improve light extraction, provide more freedom in structural engineering and also to decrease the efficiency droop [5]. However, the current injection in these nanostructured DHJs are not well adapted. When the LED is biased, the minority carrier diffusion may transport carriers over the active region. This leads into leakage current and, thus decreasing the efficiency of conventional LEDs. In addition, in the case of nanowires, with conventional current injection the nanowires need to be contacted on both ends to enable current through the device. Also, with surface plasmons the required distance between the plasmon grating and the light emitting region should be short, not more than tens of nanometers. This limits the thickness of the topmost layer drastically. [8] These requirements lead to difficulties when fabricating nanostructured DHJs and hinders the development of LEDs based on nanowires and surface plasmons.

Riuttanen *et al.* have demonstrated an alternative current injection method based on bipolar diffusion. These diffusion injected LED, *i.e.*, DILED, structure represent a new device design where, unlike conventional LEDs, the active region is located outside the p-n junction. The current injection to the active region occurs by diffusion of electrons and holes that enter the active region from the same side. Recombination creates a drain in the active region maintaining the gradient in carrier density. The demonstrated structure can help overcome the challenges in current injection, as well as in the fabrication process, in LEDs based on near surface QW structures or nanowires. [8] Three different types of DILED structures were fabricated. The two of them had a MQW stack as an active region buried under the p-n junction, while the third structure had a single QW as an active region on top of the p-n junction. Illustration of a possible solution using nanowires as light emitting region utilizing DILED structure is presented in Figure 9. The drift (solid line) and diffusion (dashed line) currents for electrons (blue) and holes (red) are also demonstrated. One should notice that with bipolar diffusion, the top contact for nanowires is not needed. This would also be the case in near surface based LEDs, *e.g.*, with surface plasmons.

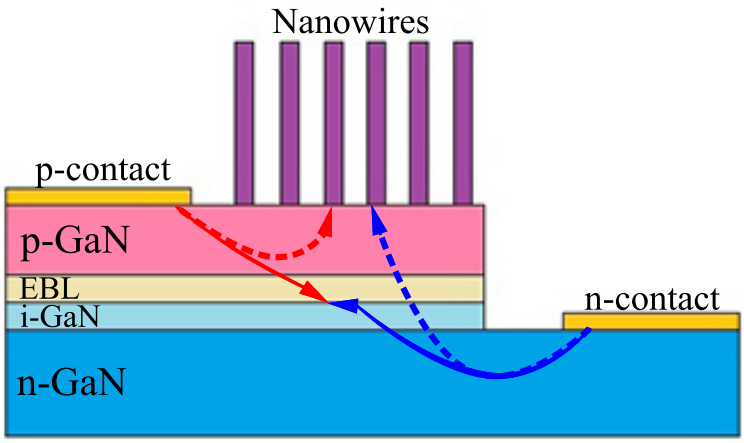

Figure 9: Illustration of a possible DILED solution using nanowires for light emission utilizing bipolar diffusion. Drift (solid line) and diffusion (dashed line) currents for electrons (blue) and holes (red) are showed. With such a desing, no top contact is needed for nanowires.

4 Experimental

In this section the growth and measurement methods, which were used in this thesis, are explained briefly. All DILED structures, as well as the reference LED, were grown by using MOVPE. Luminescence properties of the DILED structures were studied via EL, with and without temperature control, PL and μ-PL.

4.1 Metalorganic Vapor Phase Epitaxy

Metalorganic vapor phase epitaxy (MOVPE), also known as metalorganic chemical vapor deposition (MOCVD), is a chemical vapor deposition (CVD) method of epitaxial growth especially for III-V compound semiconductor structures, such as GaN. In epitaxial growth the deposited layer copies the crystalline information from the seed crystal of the material, *i.e.*, the substrate. Thus, the crystal lattices of the film and the substrate should be identical or at least closely matching. The technique behind MOVPE is that the metalorganic precursors in the gas phase are transported to a heated substrate by a carrier gas in a constant temperature forming thin film layers. The most important metalorganic compound sources in MOVPE process are trimethylgallium (TMGa), trimethylaluminum (TMAl) and trimethylindium (TMIn) [34]. For the growth of GaN, TMGa and ammonia (NH_3) precursors and for p-type doping bis(cyclopentadienyl)magnesium (Cp_2Mg) are typically used.

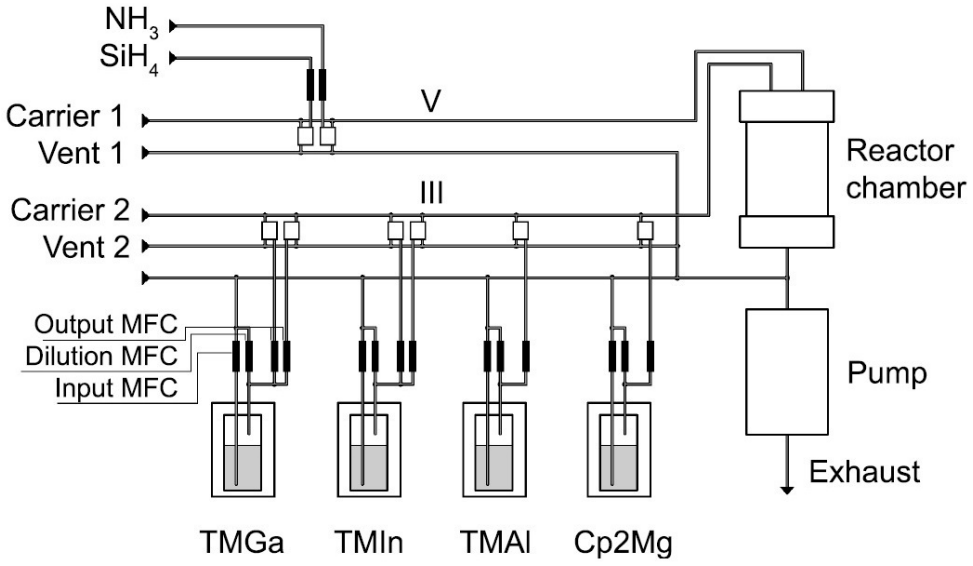

Figure 10: Schematic illustration of the gas lines of a MOVPE reactor. [35]

The major mechanisms for the MOVPE growth process are thermodynamics, kinetics, hydrodynamics and mass transportation. Because MOVPE is an exothermic process, the driving force of the growth rate depends on the thermodynamic process, while kinetics controls the rate at which reactions occur. Hydrodynamics describes the mass transport of precursor materials to the surface of the substrate. [36]

In Figure 10 a schematic illustration of a MOVPE reactor is presented. The liquid metalorganic precursors, located in steel cylinders called bubblers, is kept at constant temperature. Because the vapor pressures of precursors are highly sensitive to temperature, an accurate temperature control is needed for the bubblers. Also the precursors must not react with other gases within the system. A carrier gas, typically hydrogen or nitrogen, is bubbled through the liquid so that the precursor vapors can be carried along by the carrier gas stream. An important part of the gas flow is the desired amount of concentration of the precursors, which is why the gas flows are controlled with valves and with electronic mass flow controllers [35]. For optoelectronic devices, a constant delivery of source material is a crucial part of the process [34]. In the reaction chamber, where the substrate is located, the introduced gases are mixed and heated and a pyrolysis reaction occurs. The introduced gas phased metalorganic precursor and carrier gas interact with the heated substrate by decomposing and donating their atoms to the growing layer of the substrate.

MOVPE is a valuable tool for its suitability for mass production. There is a wide range of commercial devices grown by using MOVPE, because of its high growth rates, versatility and repeatability. These devices include lasers, LEDs, solar cells, heterostructure bipolar transistors, and high-electron-mobility transistors (HEMTs). [34, 36]

4.2 DILED Device Fabrication Process

Two different types of buried DILED structures, with a MQW stack as an active region under the GaN p-n junction, was fabricated. For convenience the structures will be referred as "Sample A" and "Sample B". In Sample A is 5 QWs in the MQW stack, Ti/Au n-contact and Ni/Au/Ti/Au p-contact pad, and in Sample B is 3 QWs in the MQW stack each with different indium compositions, Ti/Al n-contact and Ni/Au/Ti/Al p-contact pad. Otherwise the structures are similar. Both samples were grown on a c-plane sapphire substrate by MOVPE. First, a 3 µm thick unintentionally doped GaN (i-GaN) buffer layer was grown on the substrate followed by either a 5 or 3 well InGaN/GaN MQW active region. After that, a 100 nm Si-doped n-GaN layer, a 30 nm thick i-GaN spacer, Mg-doped p-type AlGaN/GaN EBL and a 400 nm Mg-doped p-GaN layer was grown.

The precursors for the aluminum, gallium and indium during growth by MOVPE were TMAl, TMGa and TMIn, respectively. For the n-type doping disilane (Si_2H_6) and for p-type doping Cp_2Mg were used. On Sample B the flows of TMGa and TMIn were same for all QWs, but the temperature was varied in order to obtain different indium compositions in QWs. The bottommost QW growth temperature was 790 ^{o}C, middle QW 810 ^{o}C and the topmost QW was 830 ^{o}C. After the MOVPE growth, the wafers were patterned with standard lithography techniques to form contact pad regions and a fingered comb-like mesa structure. Figure 11 presents an illustration of the fabricated buried MQW DILED (a) structure and (b) cross-sectional view including the drift (solid line) and diffusion (dashed line) currents for electrons (blue)

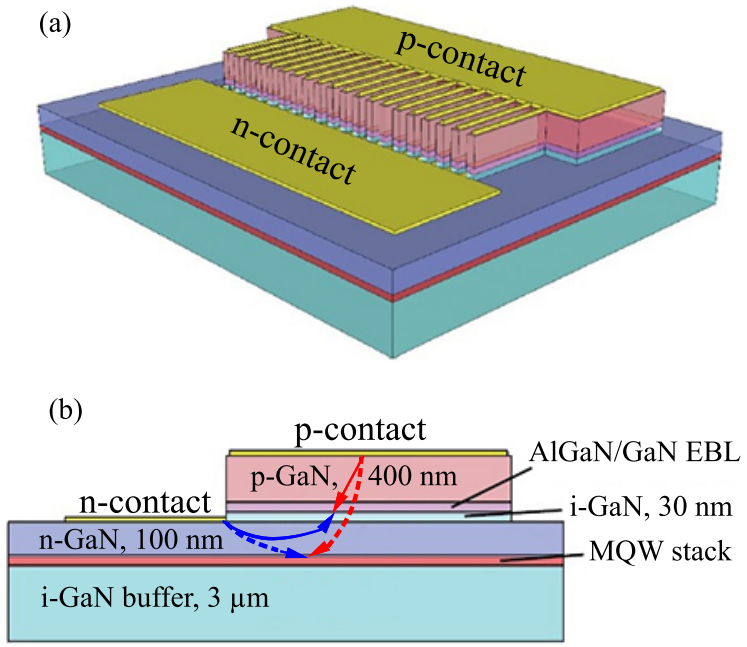

Figure 11: Schematic illustration of the fabricated buried DILED structure (a) in 3-D perspective and (b) cross-sectional view with drift (solid line) and diffusion (dashed line) currents for electrons (blue) and holes (red). Figure is modified from Ref. 8.

and holes (red). One should notice that the active layer, *i.e.*, the InGaN MQW stack, is located under the p-n junction and that the diffusion currents are injected from the same side of the structure.

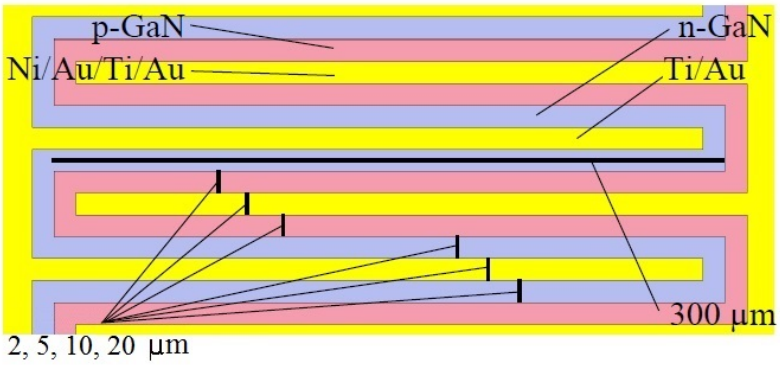

Figure 12: Schematic illustration and the dimensions of the interleaved fingers with finger widths of 2, 5, 10 and 20 µm. Figure is altered from Ref. 37.

The fabricated finger extensions were etched by inductively coupled plasma reactive ion etching (ICP-RIE) for revealing the n-GaN layer and leaving the p-GaN on top of the mesa. The number of fingers with different structures were 1, 5, 10 and 20

with widths of 2, 5, 10, and 20 µm and lengths of 300 µm. A schematic illustration of the finger structure of the buried DILED structure is shown in Figure 12. For the cathode, a titanium/gold (Ti/Au) for Sample A and Ti/Al for Sample B contact pad was patterned next to the mesa with extending fingers filling the space between the fingers of the mesa. For the p-GaN contact layer Ni/Au/Ti/Au and Ni/Au/Ti/Al were deposited on top of the mesa for Sample A and for Sample B, respectively.

Surface QW DILED

The surface QW DILED structures were also fabricated on c-plane (0001) sapphire substrates by MOVPE. The fabricated device consisted of a 3 µm thick unintentionally doped GaN (i-GaN) buffer layer on top of which a 1.3 µm p-GaN layer was grown. This was followed by a 150 nm n-doped layer, 16 nm unintentionally doped InGaN/GaN superlattice (SL) underneath layer, a 2 nm InGaN QW and a 10 nm i-GaN capping layer. The precursors were TMGa, TMIn and TMAl for gallium, indium and aluminum, respectively. For the n-type doping Si_2H_6 and for p-type doping Cp_2Mg were used.

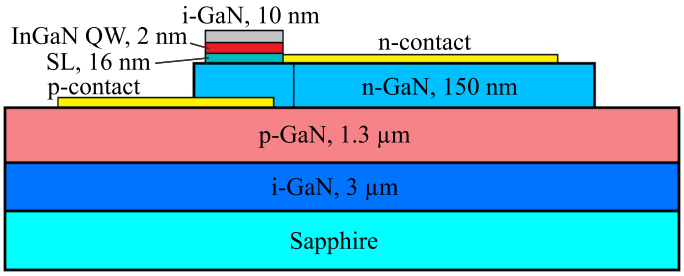

Figure 13: Cross-sectional schematic illustration and dimensions of a surface QW DILED structure.

The carrier concentrations of the layers, at room temperature, were $2 \times 10^{17}/\text{cm}^3$ for p-GaN, $5 \times 10^{18}/\text{cm}^3$ for n-GaN and $5 \times 10^{16}/\text{cm}^3$ for i-GaN. After the MOVPE growth, standard lithography techniques were used for patterning the wafers. They were etched to reveal the n-GaN layer outside the small emitter mesa region consisting of the 10 nm GaN capping, surface QW and the InGaN/GaN SL. After this, the wafers were etched using ICP-RIE to reveal the p-GaN layer outside the emitter mesa and the n-contact regions, leaving either a 2 µm or a 5 µm distance between the QW mesa and the n-contact. The n- and p-layers were contacted with Ti/Al and Ni/ITO layers, respectively, leaving also either a 2 µm or a 5 µm gap to the edges of the n-GaN mesa and to the emitter mesa. The contact pads were designed to be large squares reaching to the emitter mesa through narrow extensions for easy handling. Figure 13 presents a cross-sectional schematic with dimensions of a surface DILED structure.

Like buried DILED structures, the surface QW DILED structures are based on bipolar diffusion. The contactless surface light emitting materials are electri-

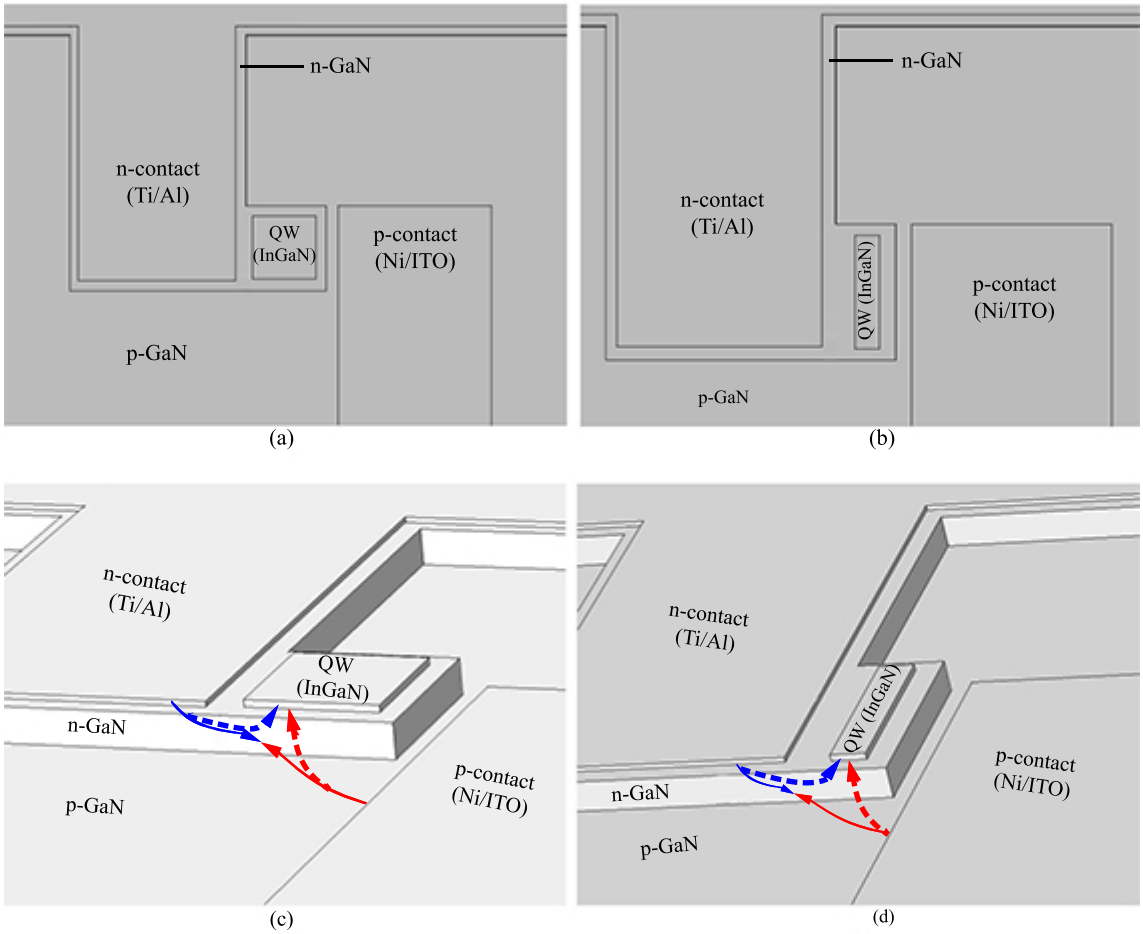

Figure 14: Illustrations of type 1 surface QW DILED structures. (a) The square QW layer from top view, (b) the rectangular shape with 10 µm width and 50 µm length, (c) the square QW layer and (d) the rectangular shape in 3-D perspective. The drift (solid lines) and diffusion (dashed lines) current for electrons (blue) and holes (red) are also visible in images (c) and (d). The 3-D models are not in scale.

cally excited by diffusion current. Unlike to the conventional DHJ structures, this approach allows to excite nanostructures located on the device surfaces without electrical contacts, forming a DHJ or absorbing layers on the device surface. This proposed method has potential when developing near surface nanostructures, such as LEDs or photovoltaic devices based on nanowires or surface plasmons. In Figures 14 and 15 are the illustrations of surface QW DILED structures with square and rectangle shapes shown. The emitter mesas were shaped as (a) 20×20 µm^2, 30×30 µm^2, 40×40 µm^2, and 50×50 µm^2 square and (b) a rectangle with 10×50 µm^2 width and length, respectively. The 3-D model heights in the figure are not in scale, *e.g.*, the length and width in the square shaped model are in the range of tens of microns while the height of the QW layer is only 2 nm. In addition, one should notice that the 10 nm i-GaN cavity layer is not shown on top of the QW for clarity in the 3-D models. The drift (solid lines) and diffusion (dashed lines) current for elec-

trons (blue) and holes (red) are shown at (c) and (d) in both figures. It is the diffusion current that is responsible for the light emission in the devices which is in contrast to conventional LEDs. In order to prevent confusion, the surface QW DILED model types will be referred as "type 1" as seen in Figure 14, and "type 2" seen in Figure 15.

As was already seen in the case of buried DILED structures in Figure 9, nanowires or surface plasmons could be adapted into surface QW DILED as well. Instead of fabricating a square or a rectangle shaped InGaN QW layer, one could deposit nanowires instead. The basic principle would be the same. No top contact would be needed and the light-emission would be due to the diffusion current.

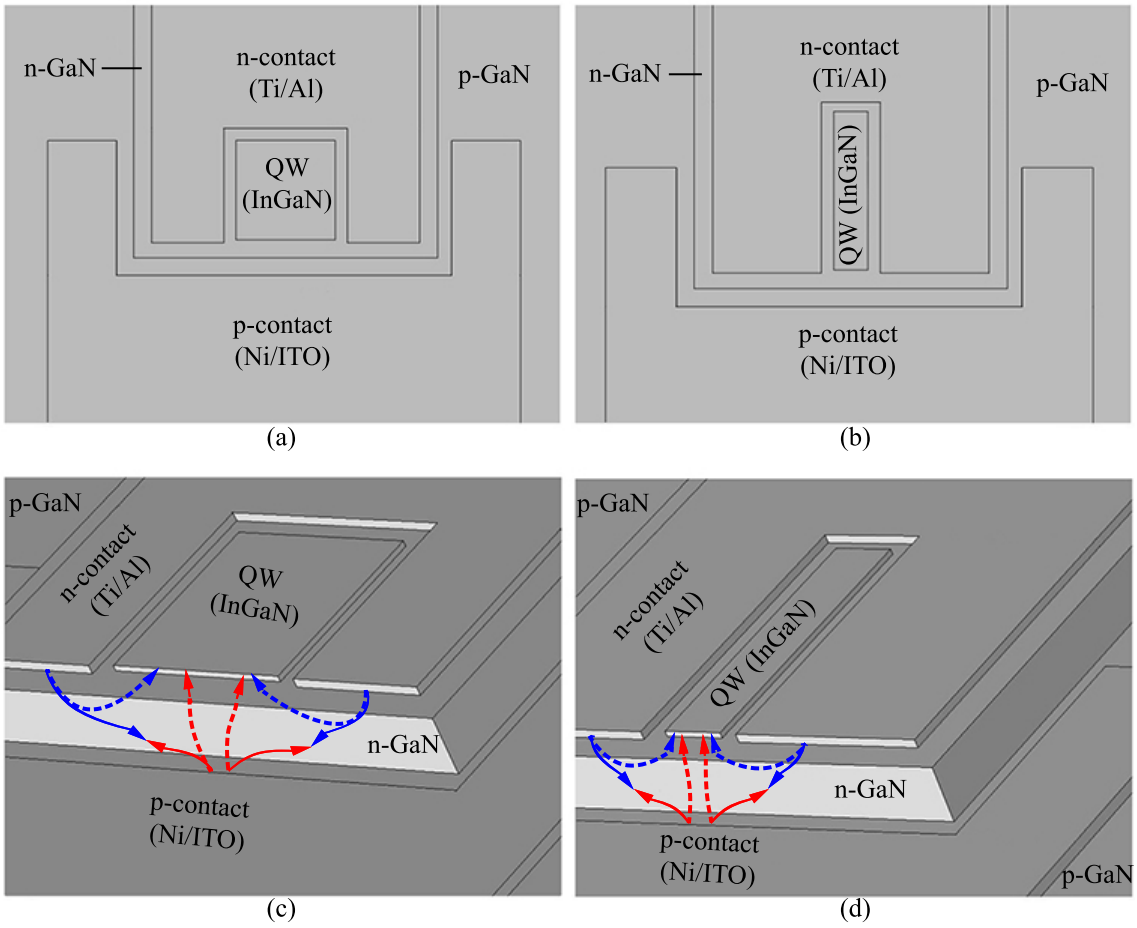

Figure 15: Illustrations of type 2 surface QW DILED structures. (a) The square QW layer from top view, (b) the rectangular shape with 10 µm width and 50 µm length, (c) the square QW layer and (d) the rectangular shape in 3-D perspective. The drift (solid lines) and diffusion (dashed lines) current for electrons (blue) and holes (red) are also visible in images (c) and (d). The 3-D models are not in scale.

4.3 Electroluminescence

Electroluminescence (EL) is an electro-optical phenomenon in which a material emits light as optical output in response to the passage of an electrical input current. The mechanism behind EL is based on the radiative recombination of electrons and holes in a semiconducting material. Figure 16 presents an illustration of the used EL setup. A source meter was attached to the probe needles and the studied sample was placed on top of an integrating sphere directly under the microscope. The emissions of the LEDs were measured at room temperature with direct current directly from the wafer without dicing them in the case of Sample A and the reference LED. Sample B and surface QW DILED wafers were diced into chips. Only back side emission was measured in each case. The integrating sphere was attached with fiber into a spectrometer and from there to a computer. The microscope images were taken with an appropriate camera.

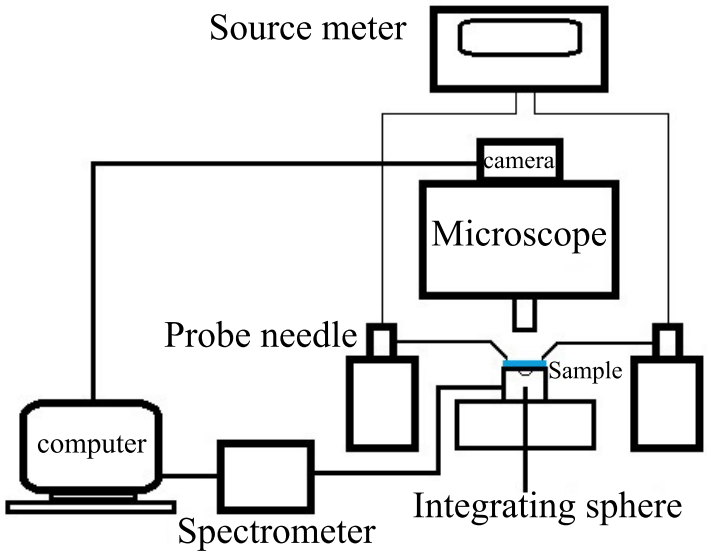

Figure 16: Illustration of the used EL setup. Back side emission were measured using an integrating sphere attached to a spectrometer. Microscope images was taken with an appropriate camera.

Temperature Controlled EL

Temperature controlled EL measurement was performed in order to study the dependence of the optical output power on temperature. The studied wafer, Sample A or Sample B, was diced into chips and attached onto a thermally conductive substrate. The attached chip was connected onto the contact pads of the thermal substrate using wire bonder with aluminum wire of 25 µm diameter. The substrate, with a DILED chip on it, was attached to a temperature controlled Peltier element plate. The temperatures used in the measurements varied from 0 ^{o}C to 100 ^{o}C with 20 ^{o}C steps. The DILED was driven with pulsed current with repetition rate of 10 kHz

and duty cycle of 10 %, which corresponds to 100 µs on-pulse widths. This was done in order to prevent the increased temperature due to Joule heating caused by electrical current. Used injection currents ranged from 20 mA to 100 mA using 20 mA steps. The optical output power was measured from the front side of the chip with an optical fiber connected to a spectrometer.

4.4 Photoluminescence

Photoluminescence (PL) spectroscopy is a simple, versatile, contactless, nondestructive technique for the investigation of electronic structure of materials. The investigated structures are excited optically at room temperature. When the incident light, *i.e.*, laser in this case, with sufficient energy hits the material, photons are absorbed and electronic excitation occurs. When these excitations relax and the electrons return to the ground state, radiative recombination occurs, thus emitting light. The emission spectrum from the PL can be used, *e.g.*, to identify surfaces, impurity levels and interface roughness of the studied material. Also, the intensity of the PL provides information on the quality of surfaces and interfaces.

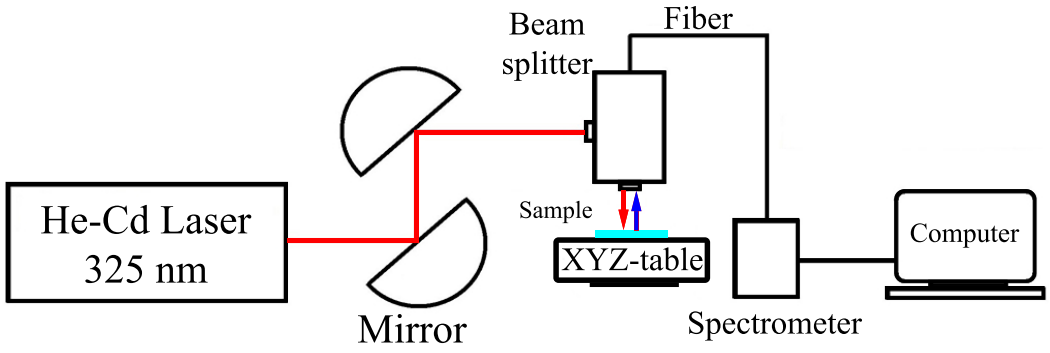

Figure 17: Illustration of the used PL setup in this thesis. He-Cd laser is reflected through the mirrors into the studied sample via beam splitter. The emitted light from the activated sample is guided into the spectrometer through the beam splitter via optical fiber and analyzed in the computer.

The required tools for an ordinary PL setup are modest. Figure 17 shows an illustration of a typical PL arrangement also used in this thesis to carry out the measurements. Measuring the continuous wave of PL intensity and spectrum is quick and straightforward in such a setup. Sample preparation is minimal, because the measurement does not rely on electrical excitation, making the PL attractive for materials with poor conductivity or contacts. In order to excite the studied structure, a sufficient energy is needed, as described in Eq. 2, and thus the penetration depth of the incident light depends on the wavelength of an incident light. In this study a He-Cd laser of 325 nm wavelength was used. The incident laser beam, red arrow in Figure 17, was reflected using mirrors and guided into a beam splitter. Through the splitter, the laser beam was focused on the studied sample (buried DILED, surface

QW DILED or reference LED), which was on top of the XYZ-table. The sample began to emit light, blue arrow in Figure 17, which went through the beam splitter and was collected through an optical fiber into the spectrometer, which was attached into a computer. All studied structures were measured from the front side of the diced, or undiced, chip at room temperature.

PL analysis is a valuable tool in the characterization of surfaces, but is highly reliable on radiative processes. The material is required to be a direct band gap material in order to emit light. It is not impossible, but materials with poor radiative efficiency, such as indirect band gap semiconductors, are difficult to study via PL.

Micro-photoluminescence

In a micro-photoluminescence (μ-PL) setup, the studied sample is excited with a laser beam focused by a microscope, which also collects the luminescence. In this thesis, a scanning near-field optical microscope (SNOM), using confocal configuration, was used to carry out μ-PL measurements. Figure 18 shows a simplified illustration of the measurement setup. The used laser of 403 nm wavelength travels through an optical fiber to the SNOM microscope. Because no probe needle was used, which is typical for SNOM, the laser beam was focused through the microscope lens passing to the sample. The continuous wave of incident laser excites the sample and the emitted light is collected, analyzed and send to the computer through an optical fiber on top of the SNOM. Also, an appropriate filter was used to exclude the reflections from the metal contacts of the structures.

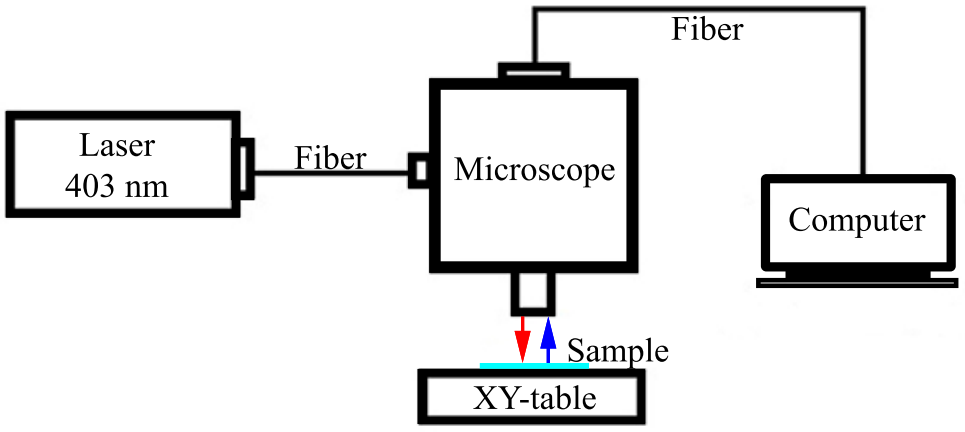

Figure 18: Simplified illustration of μ-PL measurement setup. A 403 nm laser emits a beam through an optical fiber into the microscope in which it is focused and guided onto the sample. The activated sample begins to emit light, which is collected and then analyzed by the computer.

5 Results and Discussion

In this chapter the luminescence properties of a conventional LED, buried DILED and surface QW DILED structures are presented. First, the measurement results for the conventional LED are briefly studied to provide some reference values to compare the results from the novel structures. Second, the results for Sample A DILED structures are presented, followed by Sample B DILED and finally the surface QW DILED structures. The section is concluded for the results of the PL measurement for all the studied structures mentioned above.

5.1 Conventional Reference LED

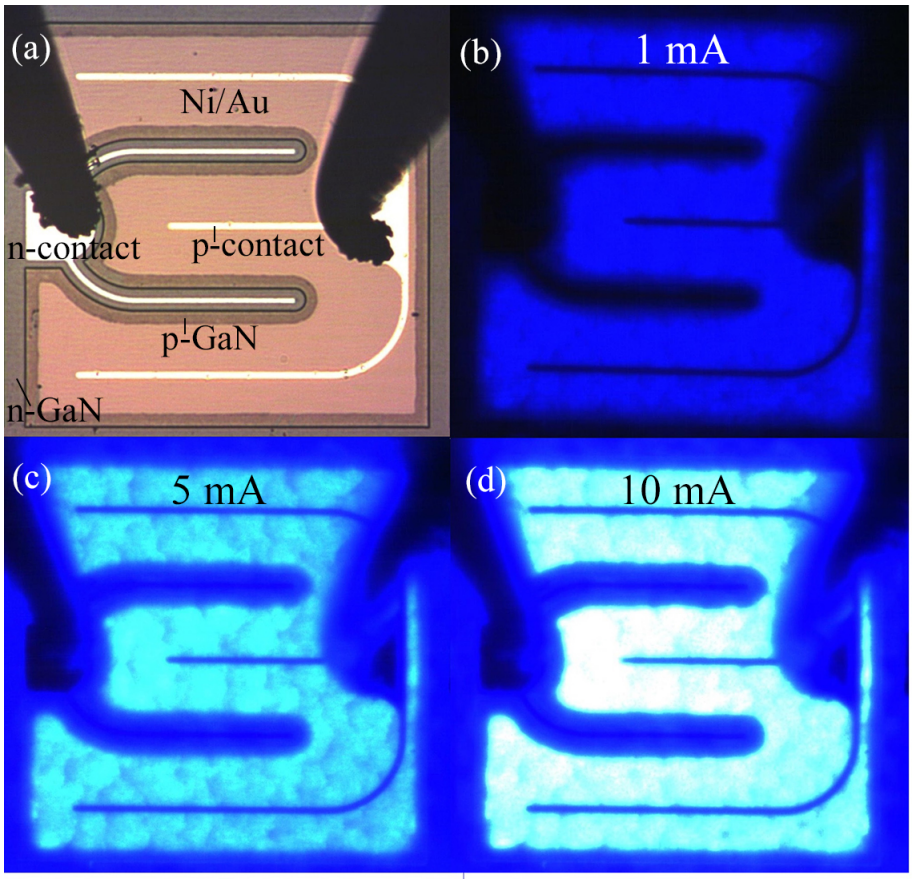

Figure 19: Microscope images of a conventional reference LED at room temperature in EL measurement (a) with no injection current and with currents of (b) 1 mA, (c) 5 mA and (d) 10 mA.

Figure 19 shows the microscope images of the conventional reference LED at room temperature EL. In (a) is the actual structure with locations of p- and n-contacts, as well as p- and n-GaN. The wide light brown area, Ni/Au, is a transparent CSL on top of p-GaN layer. The InGaN active layer is in between the p- and n-GaN like in any other conventional LED. The LED with 1 mA, 5 mA and 10 mA injection

currents are shown from (b) to (d), respectively. It can be seen that the emission is spread throughout the device smoothly because of the CSL.

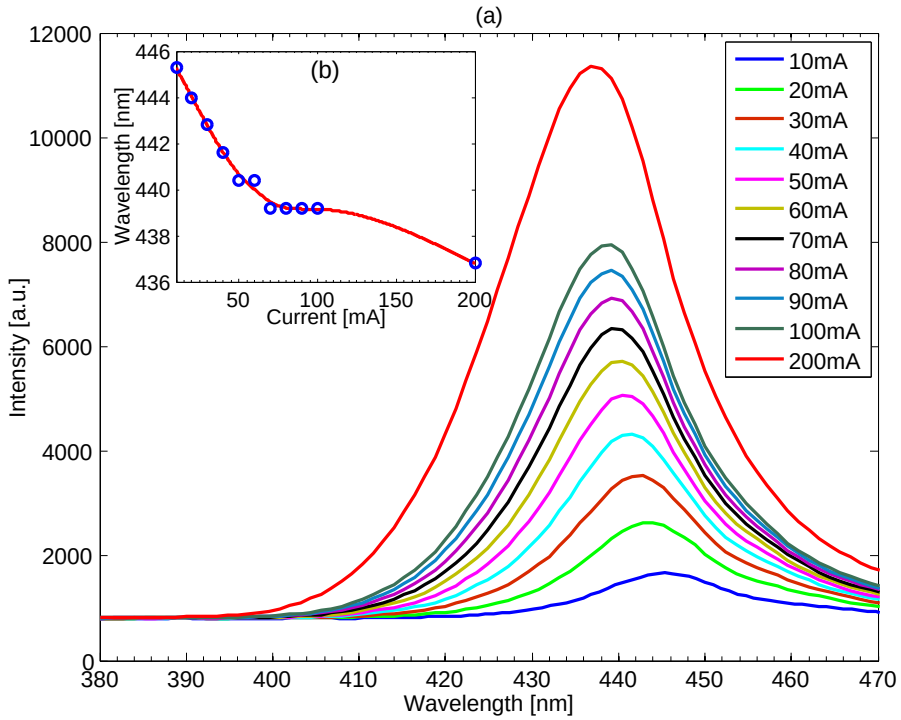

Figure 20: (a) EL measurement result for the reference LED at room temperature and (b) the corresponding blueshift in the inset of the figure.

The EL measurement result for the conventional reference LED at room temperature is presented in Figure 20. The measurement ranged from 10 mA to 200 mA. It can be seen that with lower currents, below 50 mA, the amount of intensity increases slightly more than with current above 50 mA up to 100 mA. The device emitted mainly with peak wavelength of 439 nm. However, with increasing injection current, the emission shifts to lower wavelengths as can be seen in the inset of Figure 20. The device begins to emit with peak at 445 nm under 10 mA, but the corresponding peak is shifted to 437 nm under 200 mA. This phenomenon is called a blueshift which occurs with an increased injection current and is typically observed with InGaN/GaN MQW LEDs [38, 39] and laser diodes [40]. The blueshift seen from the EL measurement may be explained by the QCSE resulting from piezoelectric fields induced by the lattice mismatch [38, 39] or from a band filling effect of the localized states by excitons [38, 41].

Typical figure of merit values, including (a) current-voltage (I-V) curve, (b) EQE and (c) optical output power, are presented in Figure 21 for the reference LED. The result of I-V characteristics in (a) is typical compared to other diodes (not shown) with threshold voltage approximately at 2.9 V. Above this voltage, the device begins to emit light and rapidly to conduct current linearly. The peak EQE value of the

LED in (b) was approximately 3.7 % with 20 mA current. It can be seen how the value of EQE first rises with currents up to 20 mA and begins to drop by further increasing the current. This is common behavior for GaN based LEDs. With injection current of 140 mA the EQE was decreased to 1 %. Optical output power in (c) was approximately 4.3 mW at 140 mA. It can be seen how with low injection current the power rises rapidly, but slows down with higher currents. The reason for the decrease in both EQE and optical output power is due to the efficiency droop. Lastly, another typical value to consider is the power efficiency, also known as the wall-plug efficiency, η, which is defined as

$$\eta = \frac{optical\ output\ power}{electrical\ input\ power} \tag{4}$$

The wall-plug efficiency for the reference LED was approximately 1.6 %. These figure of merit values were relatively low compared to those of commercial LEDs with wall-plug efficiency of 84 % and EQE of 80 %. However, all of the values mentioned above, acts as reference values for the novel LED structures studied in the next sections. One should notice that the reference LED was not diced and thus no temperature controlled EL was carried out.

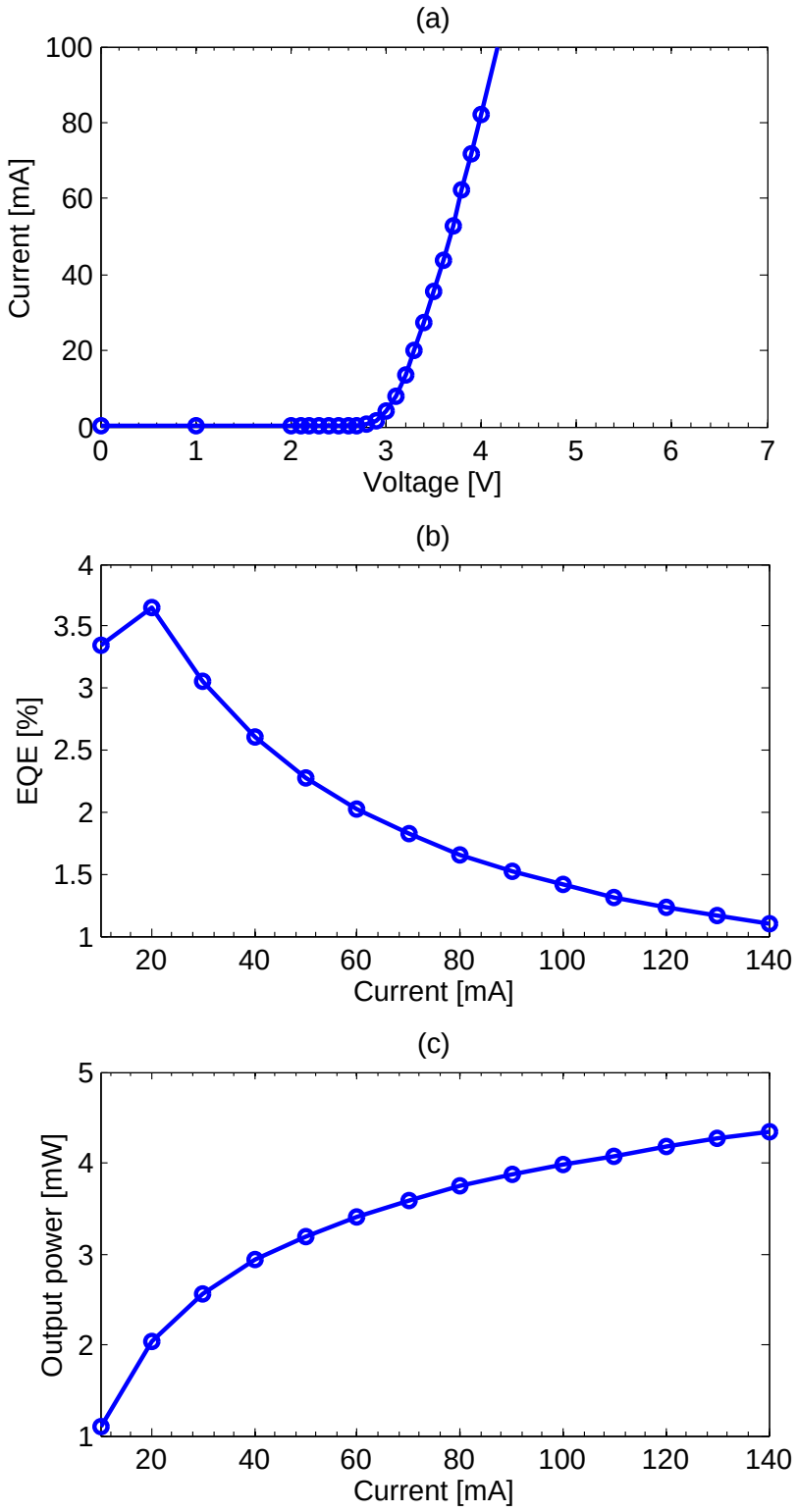

Figure 21: (a) I-V charasteristic, (b) EQE, and (c) optical output power for the conventional reference LED.

5.2 Sample A: a Buried 5 QW DILED

Figure 22 shows microscope images for Sample A DILED structure with 20 fingers and 10 µm finger widths at room temperature. Image (a) shows the device with no injection current and the locations of n-GaN, p-GaN, n- and p-contact are also presented. Injection current was gradually increased with 10 mA steps from (b) 10 mA up to (f) 200 mA, but only certain currents are presented. With injection currents from 10 mA to 30 mA, there was a significant yellow luminescence visible. With injection currents above 50 mA the blue light became dominant. Using narrower finger widths (not presented) the blue light became dominant with smaller injection currents. The blue light emitted mostly from the tip of p-GaN seen in the figure with injection currents above 50 mA. With 100 mA current there is emission slightly visible at the sides of p-contact and with 200 mA the tip of p-contact became visible.

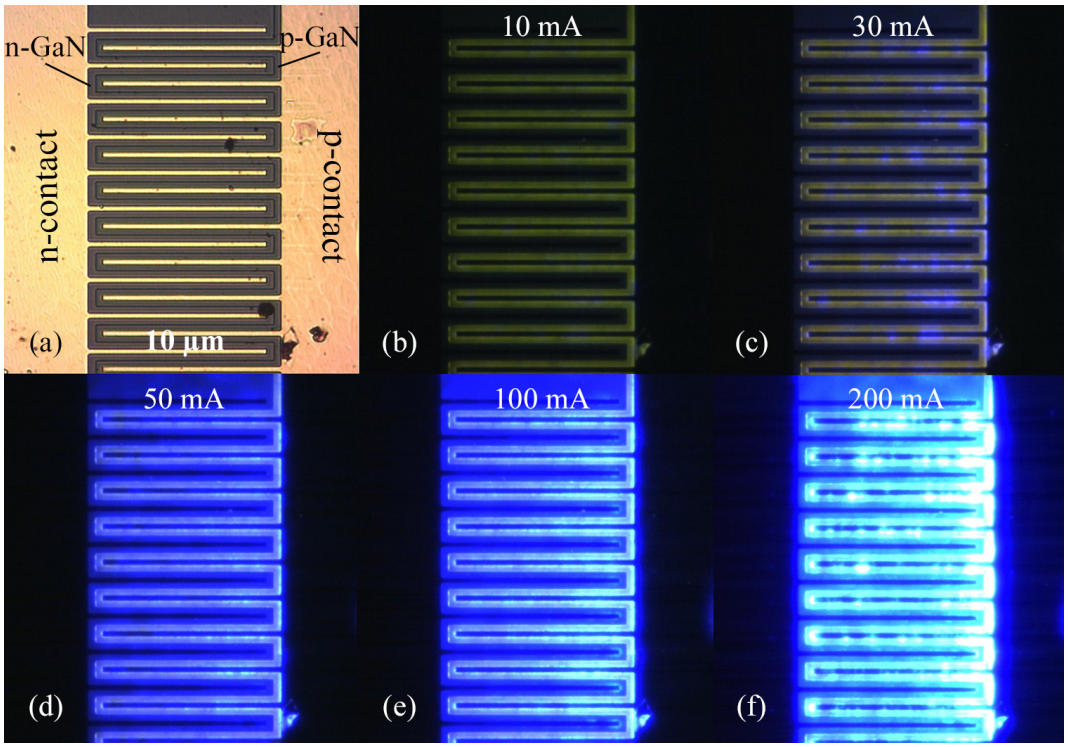

Figure 22: Microscope images of Sample A DILED structure for 20 fingers, 10 µm finger widths with (a) no injection current and with currents ranging from (b) 10 mA to (f) 200 mA at room temperature.

Figure 23 presents EL measurement results for Sample A with (a) 10 fingers and 5 µm finger widths and with (b) 20 fingers and 10 µm finger widths using logarithmic scale for intensity. In both cases the device emitted with peak wavelength approximately at 450 nm. It is not clearly visible, but closer inspection shows that both figures, with increasing injection current, shows a slight blueshift in the spectrum. In both cases the emission peak with 10 mA was at 449 nm. By increasing the injection current to 100 mA, the peak shifted to 445 nm. However, the amount of the blueshift was reduced compared to that of the conventional LED.

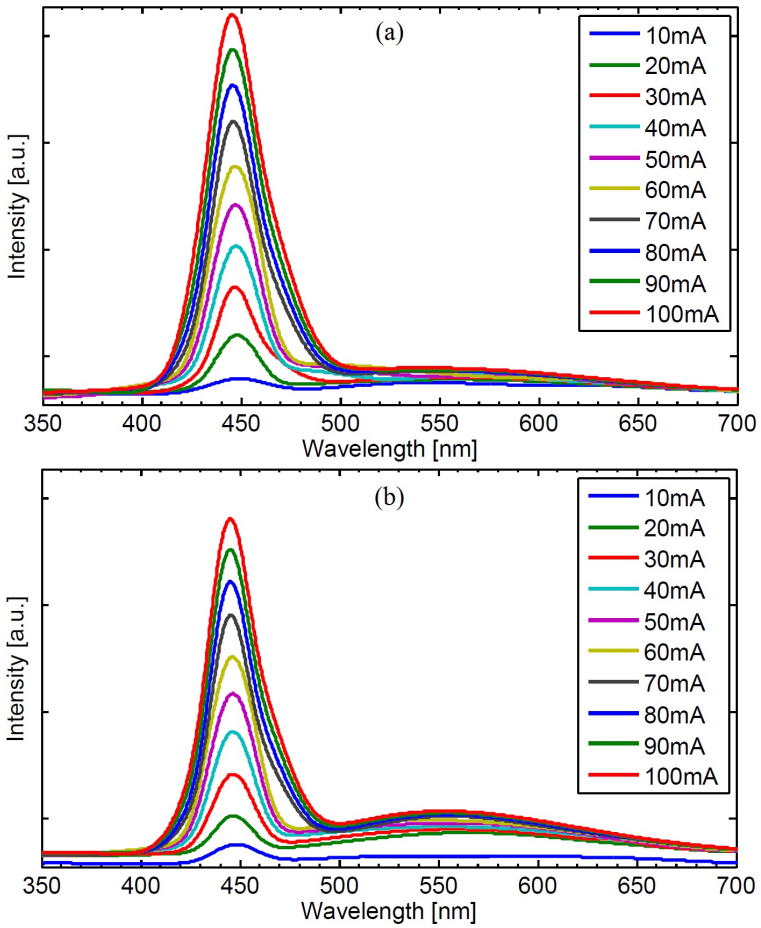

Figure 23: EL measurements for Sample A DILED structures at room temperature using logarithmic scale for intensity. The number and widths of the fingers were (a) 10 with 5 µm and (b) 20 with 10 µm.

There is also a wide spectrum visible ranging from 500 nm up to to 650 nm with highest peak approximately at 560 nm. According to Eq. 2, the corresponding band gap energy for this wavelength is $E(560nm) = 2.214\ eV$. This spectrum refers to so-called yellow luminescence (YL), a defect-induced transition which affects the efficiency of GaN based LEDs. YL in GaN is a broad luminescence band centered round 2.2–2.3 eV and has been observed in epitaxial layers grown by MOVPE, MBE and HVPE [42]. It has been reported that the origin of YL is due to Ga vacancy and related complexes in i-GaN [42, 43], shallow donor dopants, such as silicon, in n-GaN [44], and carbon impurities in i-GaN [43, 45]. YL is observed more likely from n-type GaN than from p-type GaN [42]. However, looking at Figure 22 (b) it can be seen that YL seems to emit from the mesa of p-GaN. This is most probably because of the defects in the i-GaN spacer located between the n- and p-GaN. The charge carriers are injected into the i-GaN spacer, resembling a conventional LED, and recombine through the defect states, which is why it seems like YL would originate from the p-GaN. YL is stronger with wider finger widths as can be seen from Figure 23 (b).

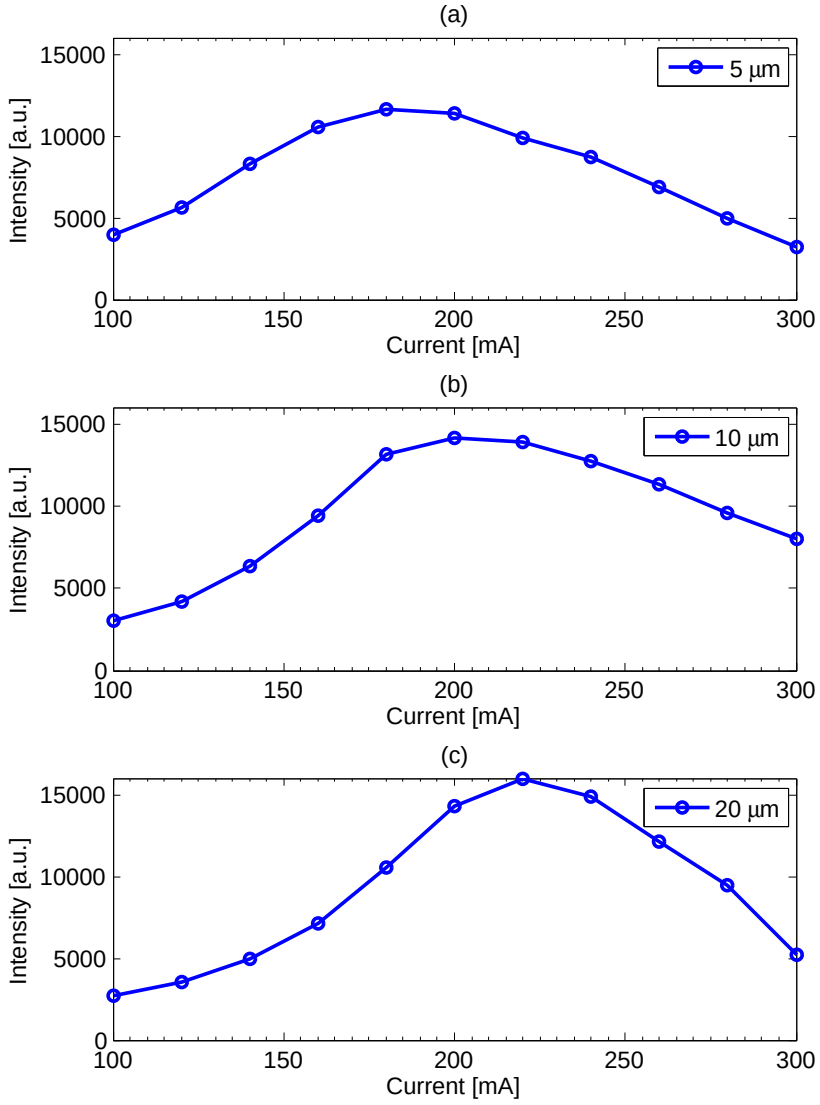

Figure 24: Intensity peaks for 5 fingered Sample A DILED structures with finger widths of (a) 5 µm, (b) 10 µm, and (c) 20 µm.

Figure 24 shows the intensity peak heights for 5 fingered Sample A with 5, 10 and 20 µm finger widths. In each case the intensity rises with increasing injection current up to a certain point. It can be seen that by increasing the width of the fingers, the maximum is obtained with higher injection current. In the case of 5 µm the maximum is reached with injection current of 180 mA while with 10 and 20 µm widths the corresponding maxima are reached at 200 mA and 220 mA, respectively. By increasing the current further from these maximum values, the emission begins to drop. The reason for this is that with increasing current the device temperature rises due to Joule heating. On the other hand, structures with wider finger widths seems to endure the heat more than with narrower widths.

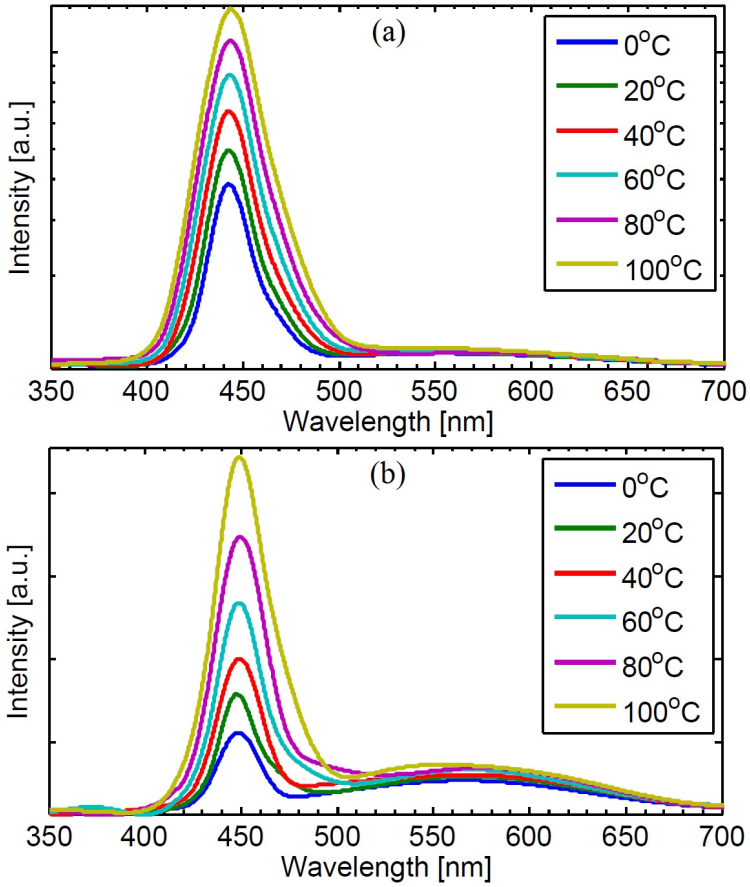

Figure 25: Temperature controlled EL measurement results with 100 mA injection current for (a) 10 fingers 5 µm width, and (b) 20 fingers 10 µm width Sample A DILED structures using logarithmic scale for intensity.

Figure 25 presents temperature controlled EL measurement results for Sample A DILED structures for (a) 10 fingers with 5 µm widths and (b) 20 fingers with 10 µm widths with injection current of 100 mA using logarithmic scale for intensity. Both spectra showed a slight oscillation which is why they were first smoothed using a Gaussian function with appropriate parameters. The origin of the oscillation is most probably interference from the cavity formed by the interfaces by the substrate/GaN and GaN/air. In both cases the intensity increased with increasing temperature. The lowest emission peak occurred at 0 ^{o}C and highest at 100 ^{o}C. This is in contrast to conventional LEDs where the increase of temperature decreases the performance of LEDs by reducing radiative recombination [18, 46], and by increasing the leakage current [47]. This abnormal temperature behavior is due to the increased diffusion current into the active region located outside the p-n junction. Again, YL with the highest peak at 560 nm, is clearly visible for wider finger width. By increasing temperature, the emission peak for YL also increased, which can be seen in Figure 25 (b).

In Figure 26 there are I-V curves presented for all measured Sample A DILED structures with (a) 1, (b) 5, (c) 10, and (d) 20 fingers with all widths, and calculated EQEs for (e) 5, and (f) 20 fingers. In general, all the I-V curves resemble the diode I-V curves, as well as the I-V curve of the measured reference LED, with threshold voltage being approximately 3 V. The actual threshold voltages varied from 2.8 V to 3.2 V. The slopes for 2 µm width are clearly much gentler than are those for other widths. The reason for this is due to unwanted parasitic resistances, *i.e.*, a series resistance and a parallel (shunt) resistance. A series resistance can occur due to excessive contact resistance [18] which causes the slope to be much gentler compared to that of a steep ideal diode (not presented). This is most probably because the quality of the DILED contact pads are not optimal. No clear effect of a shunt resistance is visible in the figure, which would be caused by surface imperfections [18] and causes the curve to rise below the threshold voltage. A closer inspection shows that in Figure 26 (d) with 20 fingers with 2 µm and 5 µm finger width, a slight shunt resistance might be present, but this can also be caused by sub-threshold turn on because of the defects.

The calculated EQEs of the Sample A DILED structures are quite low compared to the reference LED or the commercial ones ranging mainly from 0.2 % to 0.5 %. It can be seen from the figure that EQE increases with increasing injection current. In addition, with high injection currents, EQE increases much more rapidly than with lower currents. One possible reason could be that with increasing current the operating temperature at the device junctions also increases, which in turn would improve diffusion current into the MQW regions. This behavior is the exact opposite compared to the conventional LEDs seen in Figure 21 (b). It has been reported that elevated junction temperature can have a significant effect to LEDs [47] and that EQE decreases with increasing temperature [48]. In addition, due to the efficiency droop, the value of IQE decreases with increasing injection current [30] and because the EQE is directly proportional to the IQE, also the EQE decreases with increasing injection current.

Finally, Figure 27 presents the optical output power for Sample A with (a) 1, (b) 5, (c) 10, and (d) 20 fingers. Typically, the output power was in the range of 0.4 mW to 1 mW, but also over 2 mW was achieved. Comparing the shapes of these results to those of the reference LED ones in Figure 21 (c), one major observation is seen. With increasing injection current the output power of a conventional LED will be saturated into a certain value with increasing injection current. However, in all Sample A cases this phenomenon is the exact opposite. With increasing injection current the output power increases. The higher the current the more rapidly the output power rises. This is due to the increase in diffusion current with the aid of increased junction temperature as mentioned previously. The wall-plug efficiencies for Sample A DILED structures varied from 0.06 % up to 0.16 %. These values are relatively small compared to those of the reference LED and commercial LEDs. One possible reason is because the p-contacts detached during growth and the process was started over. Thus, the quality of the ohmic contacts was not optimal. However, the behavior of the EQE and optical output power makes the DILED structures

interesting with high possibilities in developing novel GaN based LEDs.

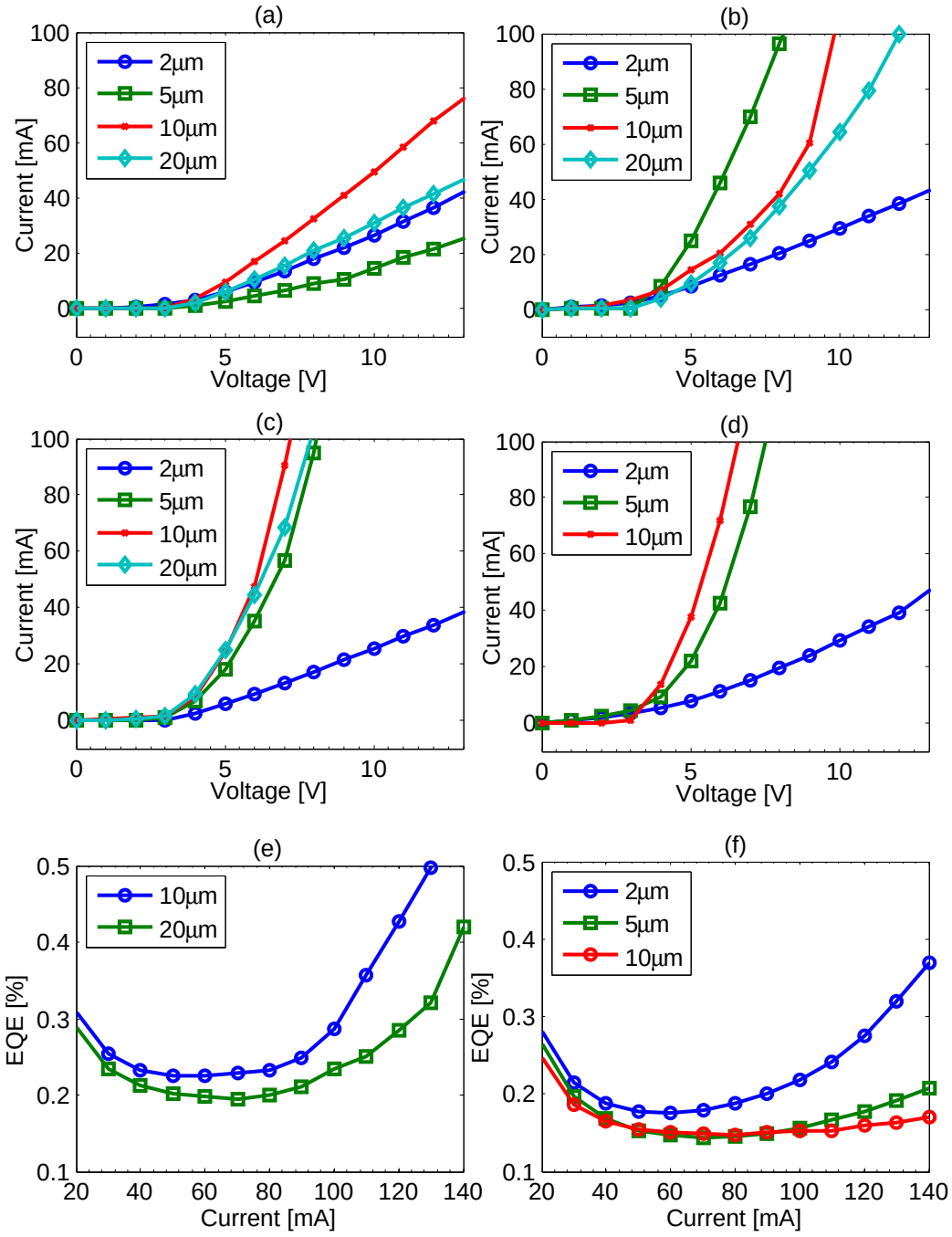

Figure 26: I-V curves of Sample A DILED with (a) 1, (b) 5, (c) 10, and (d) 20 fingers, and EQEs with (e) 5, and (f) 20 fingers.

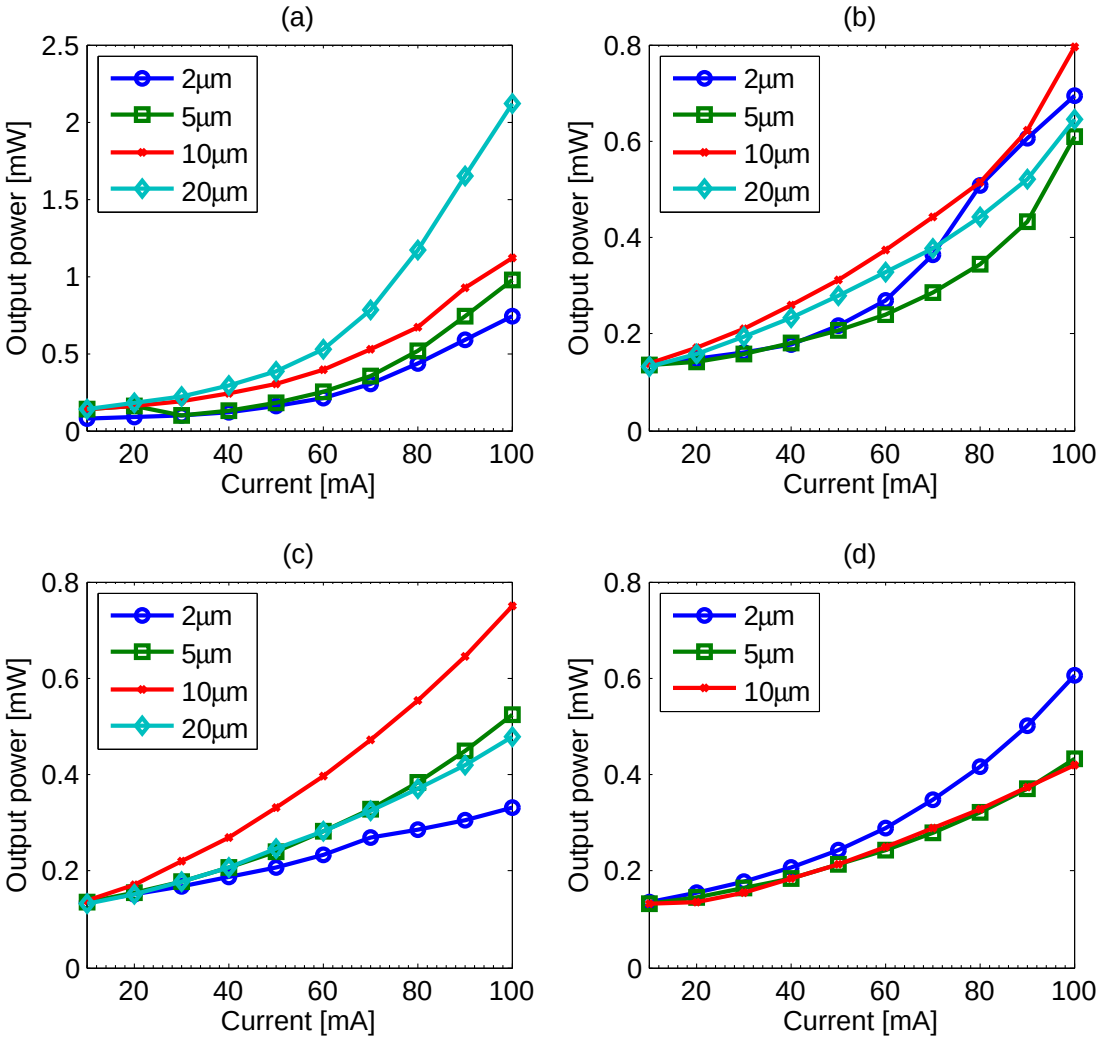

Figure 27: Optical output power as a function of current for Sample A DILED structures with (a) 1, (b) 5, (c) 10, and (d) 20 fingers.

5.3 Sample B: a Buried 3 QW DILED

Figure 28 shows microscope images of Sample B DILED structure for 20 fingers with 10 µm widths. Figure (a) shows the actual structure with no current. The device resembles the Sample A in Figure 22, but this time with p-contact on the left side and n-contact on the right side. The locations for n-GaN and p-GaN are also shown in the figure. Injection current was gradually raised from 10 mA to 100 mA, but only certain current values are shown. Compared to Sample A it is relatively difficult to observe, but there seems to be YL locations present at the tips of p-GaN. In Figure (b) with injection current of 20 mA two example locations of YL are marked with red circles. Also, the exposure time was slightly increased to emphasize the emissions and to get clearer view of YL. Like in the case of Sample A, the reason why YL seems to originate from p-GaN and not from n-GaN is due to defects in i-GaN spacer located between the n- and p-GaN where the charge carriers recombine, as was already mentioned in Section 5.2. Even with wider finger widths (not presented), *i.e.*, 20 µm, YL was relatively dim compared to those of Sample A ones. With currents above 30 mA, blue light begins to emit from the tip of p-GaN and with currents above 50 mA, also from the sides of p-contacts. The emission also slightly originates from the tip of n-GaN which can barely be seen with injection currents of 100 mA.

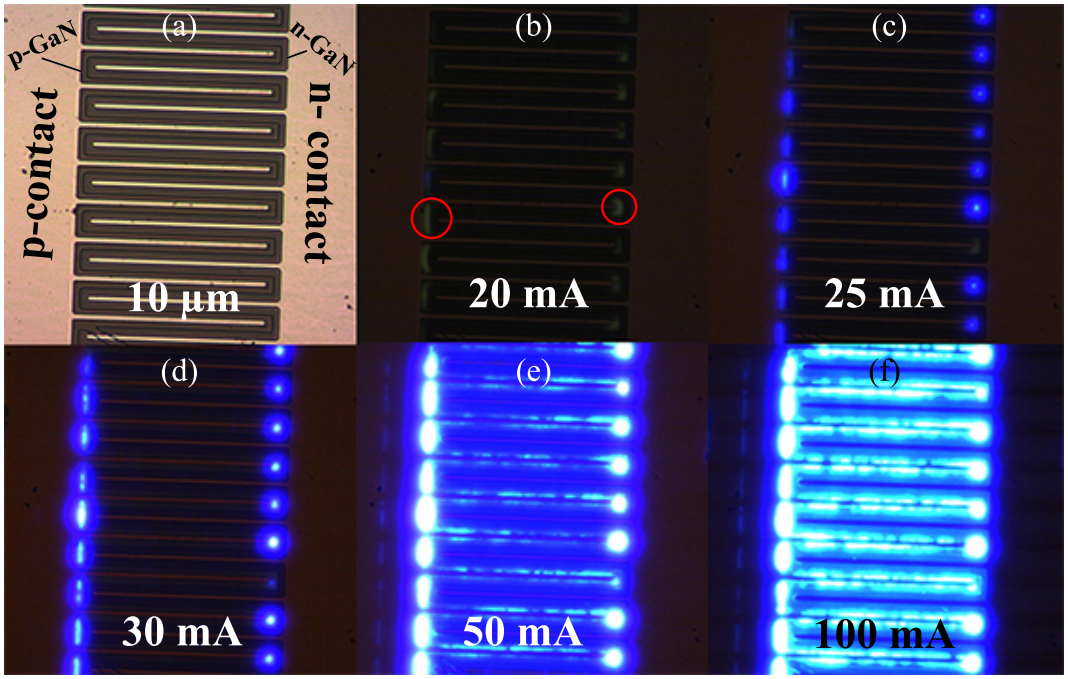

Figure 28: Microscope images of Sample B DILED structure for 20 fingers, 10 µm finger widths with (a) no injection current and with currents ranging from (b) 20 mA to (f) 100 mA. Red circles in (b) shows two example locations of YL.

Figure 29 shows EL measurements for Sample B with (a) 10 fingers with 5 µm finger widths, and with (b) 20 fingers with 10 µm widths. There are clearly two peaks visible in both cases. In the case of (a) the first peak occurs at 430 nm and

the second one at 480 nm. The first emission peak reaches its maximum at 60 mA. Above this, the peak decreases while the second peak increases gradually with all currents. Above 70 mA the second peak becomes dominant while the first peak continues to decrease.

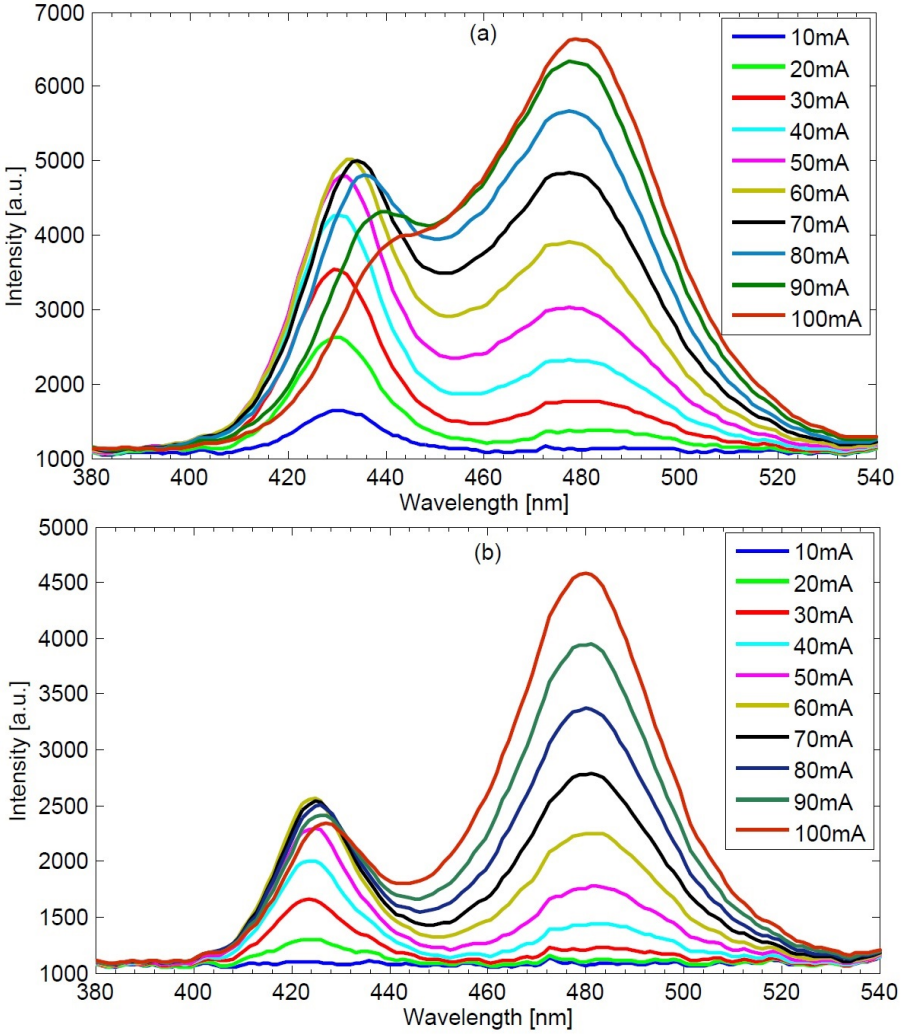

Figure 29: EL measurement for Sample B DILED structures with (a) 10 fingers 5 µm, and (b) 20 fingers 10 µm at room temperature.

The reason for the first peak to decrease above 60 mA is due to increased leakage current into the next QW, thus decreasing electron-hole recombination in the first QW region. Closer inspection reveals, that there is also a shifting to longer wavelengths visible ranging from 430 nm to 439 nm at the first emission peak, and from 478 nm to 480 nm at the second peak. This shifting to longer wavelengths during increased injection current is called a redshift and is mainly associated with junction-temperature rise in InGaN LEDs [49]. The reasons for the redshift could be due to a higher indium composition in QWs or a stronger polarization-induced QCSE [16]. This indicates that the temperature increases with increased injection

current in the structures. In addition, with high current values (not presented) the temperature due to Joule heating at ohmic contacts begins to overheat the structure, thus destroying it rapidly.

In the case of (b), the first peak is approximately at 425 nm and the second at 480 nm. The first emission peak reached its maximum at 60 mA and begun to decrease with increased injection currents due to leakage current into the next QW. The emission peak also showed redshift to longer wavelengths from 424 nm to 427 nm. The second emission peak became dominant with currents above 70 mA. Unlike in the case of (a), the second peak shows a slight blueshift from 483 nm to 480 nm with increased currents. In addition, structures with wider finger widths endured high injection currents. The structures, with narrower finger widths, were more prone to overheat and be destroyed with lower injection currents, than those with wider widths. With all studied Sample B DILED structures, with different amount of fingers and different size of widths, no significant YL emission spectra were observed during EL, thus indicating an improved quality compared to Sample A. Also, the blueshift during an increase of injection current was small compared to those of the reference LED.

Figure 30 shows temperature controlled EL measurements with corresponding intensity peaks for Sample B DILED structure with 20 fingers with 10 µm under 100 mA injection current. Again, logarithmic scale was used for intensity. There are total of four peaks visible. First at 370 nm, second at 390 nm, third at 425 nm, and fourth at 485 nm. The original curve for 485 nm peak had visible oscillation interference in the spectrum so it was fitted using smoothing spline with an appropriate parameter. According to Eq. 2 the corresponding energies for the peaks are $E(370nm) = 3.35\ eV$, $E(390nm) = 3.18\ eV$, $E(425nm) = 2.92\ eV$ and $E(485nm) = 2.56\ eV$. The first peak would refer to band-to-band transition of GaN when comparing the band gap energy to the corresponding value in Table 1. Looking at Figure 8 it can be seen that by increasing the amount of indium composition, the energy band gap decreases. Thus, the second, third and fourth peaks refer to the top, middle and bottom QWs, respectively.

Remembering that the MQW stack is outside the p-n junction (see Figure 11 (b)) and looking at the emission peaks, one can deduce that the bipolar diffusion is strong enough to transport charge carriers from the same side into the MQW stack and also to excite active region at the bottommost QW. However, some of the charge carriers recombine in the GaN interface indicated by the 370 nm emission. Majority of charge carriers are transported into the middle QW as well as to the bottommost QW passing the topmost QW, because it does not capture them efficiently. One probable reason could be that the topmost QW is much shallower compared to the other QWs. All the emission peaks reacted to temperature. The first and the fourth peak, *i.e.*, GaN and the bottom QW, increased as temperature increased, while the second and the third peak, *i.e.*, top and middle QW, decreased due to the increased leakage current into the bottommost QW. Also, redshifting to longer wavelengths from 365 nm to 370 nm and from 427 nm to 432 nm can be seen in GaN and in middle QW peaks, respectively.

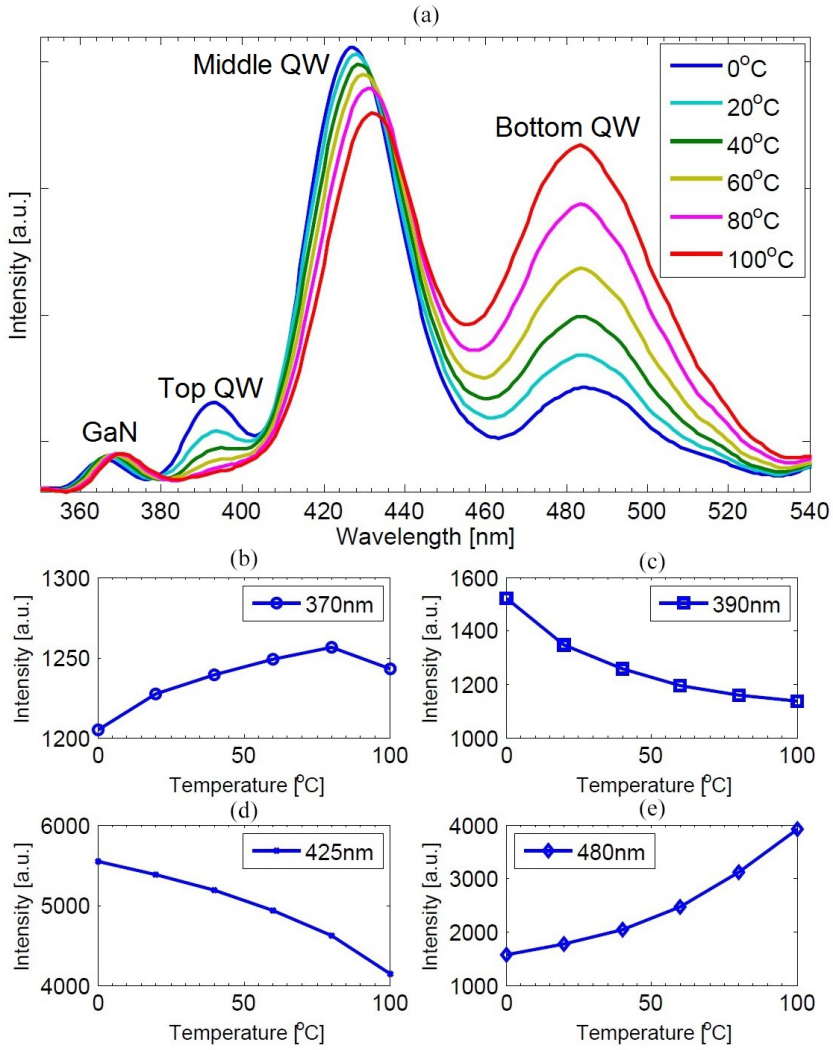

Figure 30: (a) Temperature controlled EL measurements with intensity peaks, from (b) to (e), for Sample B DILED structure with 20 fingers 10 µm widths under 100 mA injection current using logarithmic scale for intensity.

Figure 31 shows (a)–(d) I-V curves for all Sample B DILED structures, (e) few EQE curves and (f) optical output power curves. Again, all the curves resembled the diode I-V characteristic curves shown in Figure 21 (a). Relatively good diode-like characteristic occurred with 10 fingers 20 µm in (c), as well as with 20 fingers 10 µm in (d). No functioning samples with 2 µm fingers were found. The threshold voltage of Sample B structures were typically in the range of 4 V, as can be seen from the figure. This is approximately 1.2 V more than was the threshold voltage in reference LED. However, there were also some structures with threshold voltage approximately at 3.2 V, mostly with 10 and 20 fingers. In all structures, there were significant parasitic series resistances affecting the characteristics of the structures due to unoptimal contact quality. All 2 µm and 5 µm widths showed only gentle slopes, excluding in (d) with 20 fingers, while the curves with other structures were

somewhat steep. Looking at the structure of 10 fingers with 10 µm width in (c), it can be seen how the curve begins to rise much earlier than those with the other structures. As mentioned before, this is due to the other parasitic resistance, the parallel (shunt) resistance, due to excessive contact resistance and from imperfections in the fabrication process. The effect of both shunt and series resistance can be seen in (b) 5 fingers 20 µm and in (c) 10 fingers 10 µm, where first the curve begins to rise immediately above 0 V and is still a little gentle above 5 V.

The EQE values for Sample B are presented in (e). For clarity, only few structures are presented. The reason for this is firstly because there were no significant differences between different structures, and secondly EQE values dropped quickly with all other structures using injection currents above 60 mA mostly due to Joule heating. Only the structures with 10 fingers with 10 µm and 20 µm widths and 20 fingers with 10 µm widths are presented. All structures behaved similarly, at low injection currents EQE values dropped until approximately between 30 mA and 40 mA it started to rise excluding those structures that were overheated during the measurements. However, with injection currents above 70 mA all EQE values begun to decrease slightly except for the structure with 10 fingers with 10 µm finger widths as seen in the figure. Measurements above 100 mA was challenging to execute, because of the Joule heating in the structures rapidly destroyed the structures. The values of EQEs varied from 0.2 % to 0.5 %, which were approximately the same as was with Sample A, yet low compared to the reference LED and commercial LEDs.

Finally, in (f) is the optical output power presented for Sample B with different amount of fingers. Only the presented structures endured injection current up to 100 mA. These results were slightly better than those of Sample A with output powers ranging from 0.5 mW up to 1.3 mW and wall-plug efficiencies from 0.11 % up to 0.19 %. Still, these values are low compared to those the reference LED and commercial ones. However, like in Sample A, with increasing injection current the output power did not saturate like the conventional LED seen in Figure 21 (c). Both, Sample A and Sample B DILED structures, with their unique properties are potential candidates when designing LEDs based on nanowires or surface plasmons. First, the fabrication would be easier, thus providing more flexibility in device engineering, and secondly, the limitations of high-efficiency due to efficiency droop would be considerably reduced. In order to improve the efficiency of DILEDs, the dimensions of the structures, including finger widths and semiconductive layer thicknesses, as well as the carrier concentrations should be optimized. Also, the purity of the introduced materials would affect.

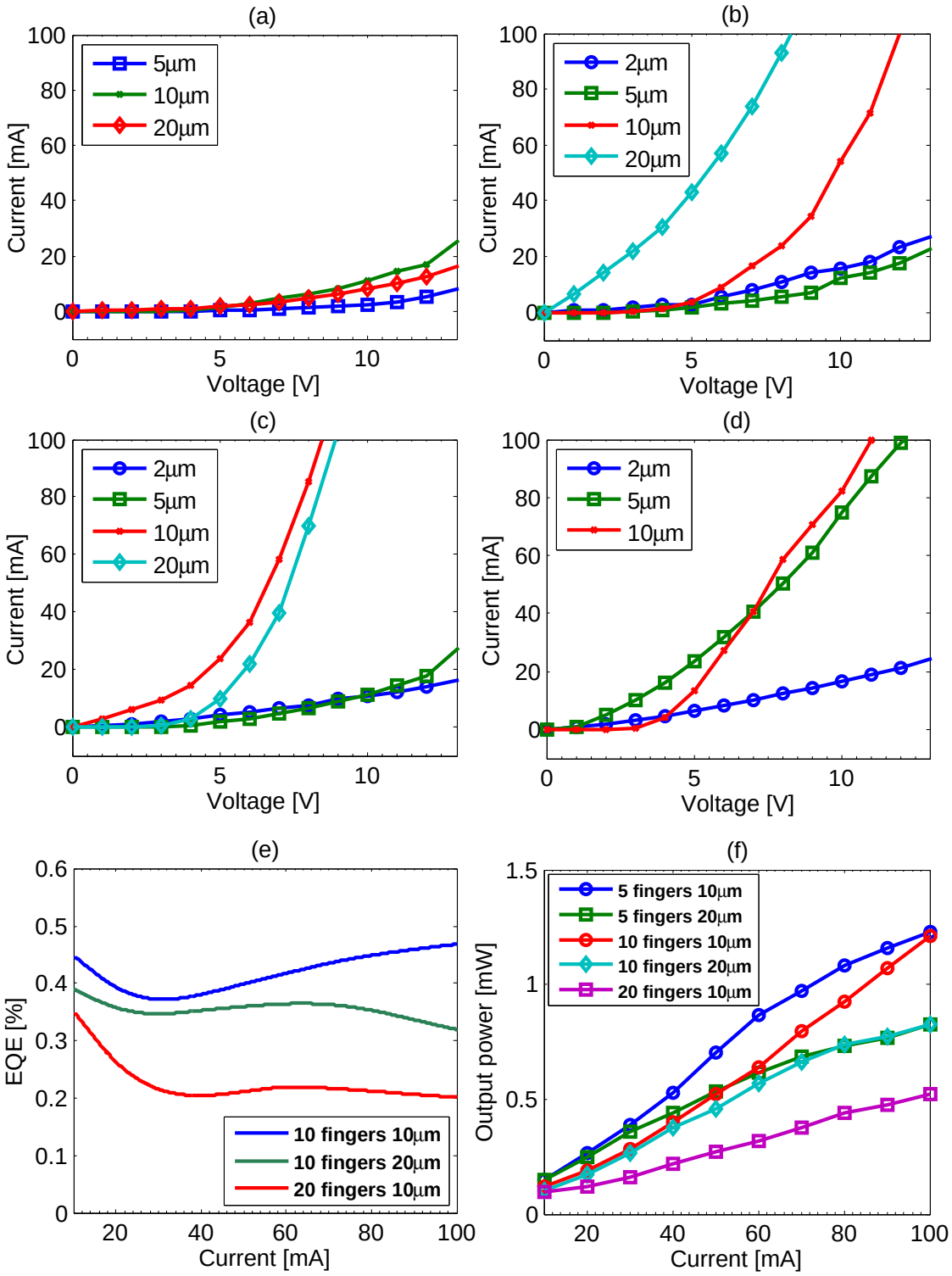

Figure 31: I-V curves with (a) 1, (b) 5, (c) 10, and (d) 20 fingers, (e) EQE curves with different fingers and finger widths and (f) optical output power curves for Sample B DILED structures.

5.4 A Surface QW DILED

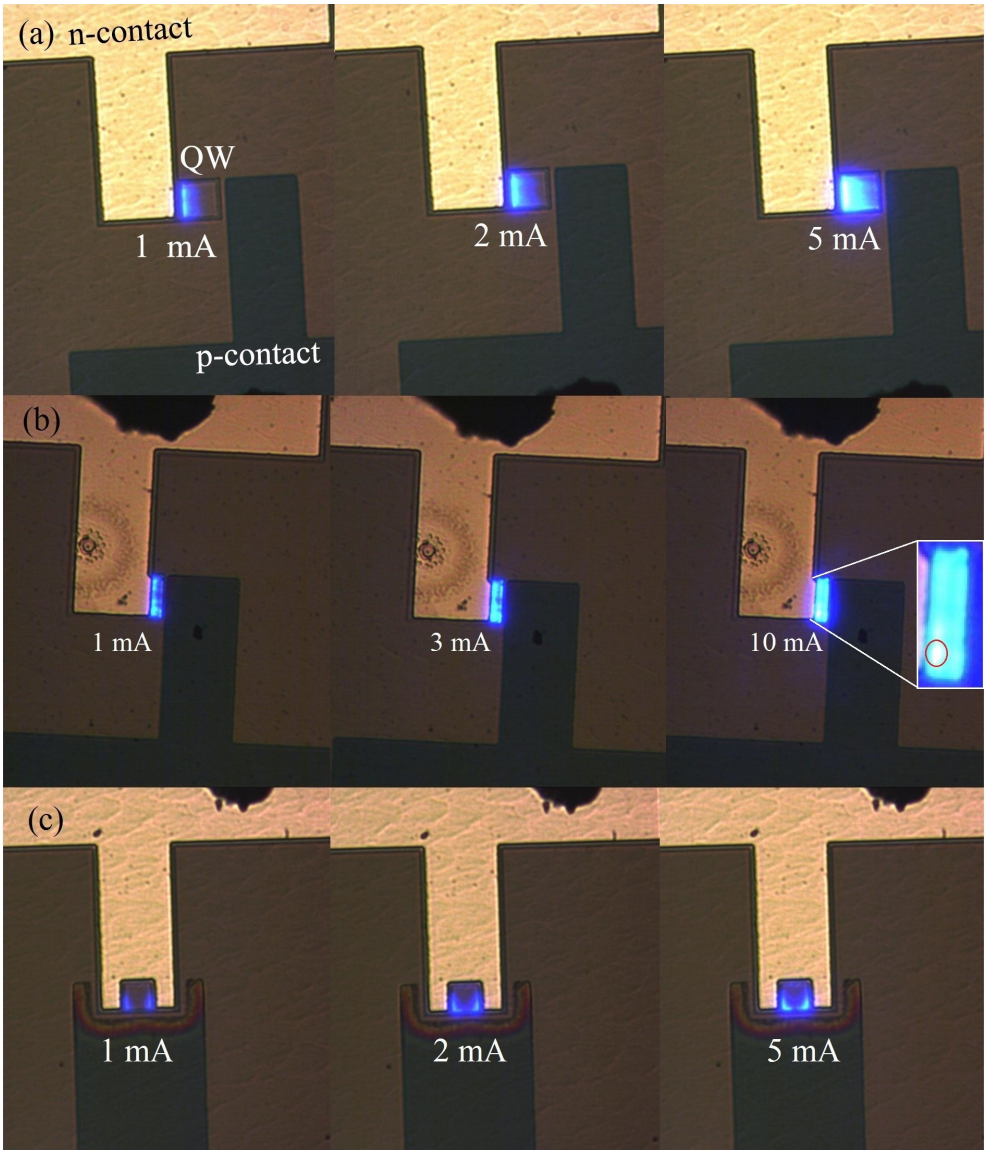

Figure 32: EL microscope images for surface QW DILED structures with dimensions of (a) type 1: 40 × 40 μm^2 / 5 μm gap, (b) type 1: 10 × 50 μm^2 / 2 μm gap and (c) type 2: 30 × 30 μm^2 / 5 μm gap. The red circle in the enlarged image in (b) indicates the location of stronger emission.

Figure 32 shows EL microscope images for three different types of surface QW DILED structures. The corresponding dimensions are (a) type 1: 40 × 40 μm^2 with 5 μm gap, (b) type 1: 10 × 50 μm^2 with 2 μm gap and (c) type 2: 30 × 30 μm^2 with 5 μm gap. The injected current was gradually raised from 1 mA up to 5 mA in the cases of (a) and (c) and from 1 mA to 10 mA in (b). Emission could also be seen with naked eyes with currents approximately above 2 mA. As can be seen from the figure, the emission begins from the n-side of the structure in the case of (a) and

(b). In the case of (c) the emission begins from the p-side corners of the square QW. In addition, by increasing injection current in the case of (b), the emission originates initially from the p-side of the QW as well. It did not matter whether the gap was 2 µm or 5 µm in each case, the behavior was identical. The only difference was that some 2 µm structures emitted more light with less injection current. Taking a closer look at (b) under 10 mA injection current, it appears that the emission is slightly stronger at the bottom of the structure near the n-contact. This is indicated at the enlarged image with a red circle. Similar behavior was also observed with several other structures excluding type 2 structures seen in (c). All structures were prone to overheat due to Joule heating. It could be seen through the microscope how the contact pads were destroyed quickly with injection currents above 10 mA. This was most probably because of the possible impurities underneath the contact pads. This indicates that there are great resistive losses due to unoptimal contact pad quality.

In Figure 33 there are some different types of surface QW DILED structures measured by µ-PL. In (a) is type 1: 10 × 50 µm^2 structure with 2 µm gap and its corresponding µ-PL result on the right. In (b) and (c) are similar structures with 30 × 30 µm^2 and 40 × 40 µm^2, respectively, both with 2 µm gap. Finally, there is the type 2 surface QW DILED structure in (d) with 30 × 30 µm^2 with 5 µm gap. The first predictions were that in the cases from (a) to (c) the emission would be brighter on the left side of the structure. This is the n-contact side, as was seen in the microscope images in Figure 32 (a) and (b), while the p-contact side would not emit as much, if at all. There appears some differences in the emission when comparing the measured µ-PL results to the corresponding EL microscope images. The emission from µ-PL should be the brightest at the edges of the n-side of the QW in the cases from (a) to (c). However, the measurements show quite different results in each case. In (a) the emission is relatively stable throughout the structure. Yet, there appears a local hot spot where the emission is highest at the bottom of the structure at the n-contact side, as was seen in the enlarged image at Figure 32 (b). However, this was not the case with other similar structures. The emission with all measured structures were different.

The 30 × 30 µm^2 structure in Figure 33 (b) shows more emission at the n-contact side like was seen in the corresponding EL microscope image. However, looking the 40 × 40 µm^2 structure at (c), the emission is more on the p-contact side. Measuring other similar surface QW DILED structures with different dimensions and gaps, nearly all behaved differently. Some emitted mainly from the n-contact side while others emitted constantly throughout the QW. Also, cases where the emission originated from the p-contact side was observed. Even though the gap at Figure 32 (a) is 5 µm does not matter, because all such structures with 2 µm gaps acted similarly. The only difference observed was that with 2 µm gaps the emission was stronger with smaller injection currents. The fact that the structure in 33 (b) resembled the behavior predicted from the corresponding EL microscope images, was probably just a coincidence. The emission was constant throughout the structure when measuring other similar structures.

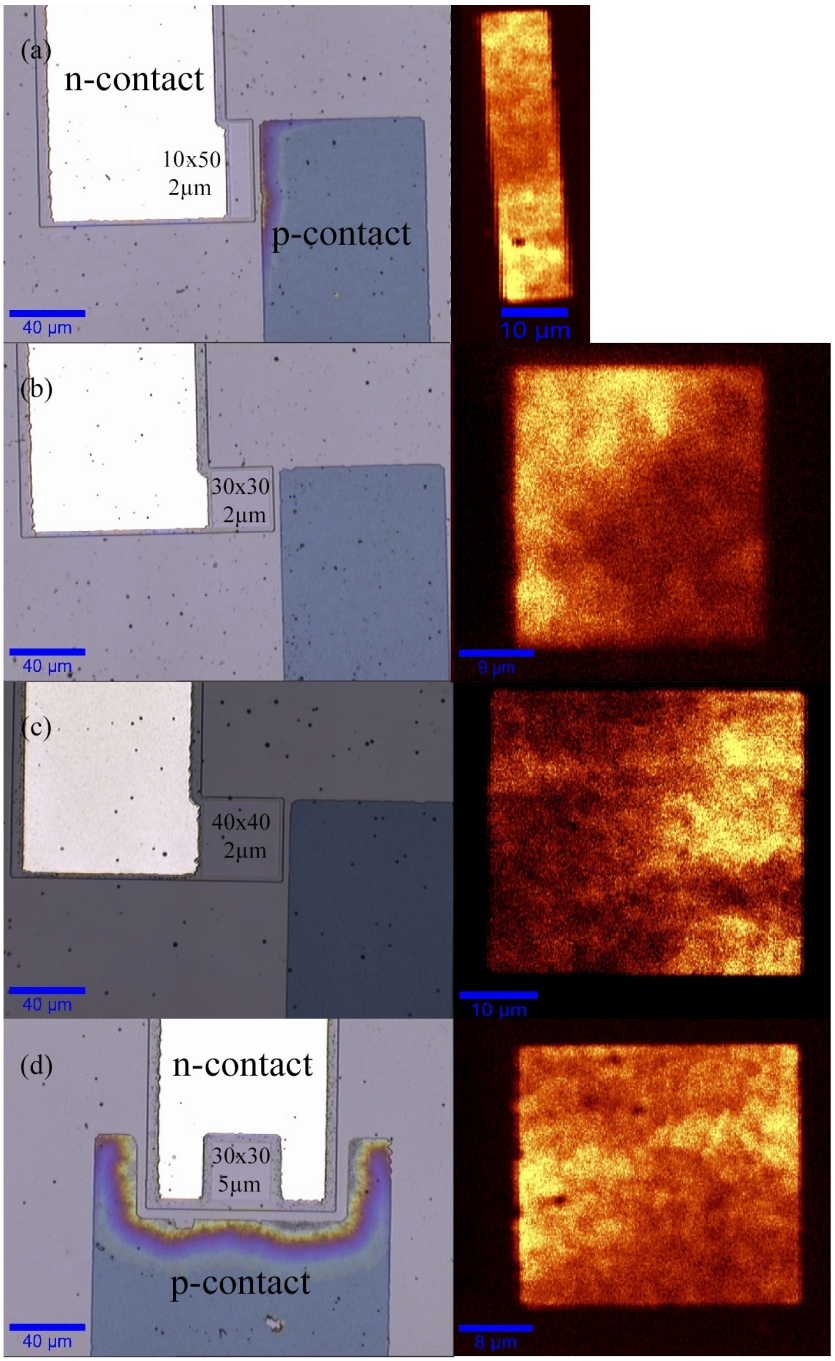

Figure 33: µ-PL measurement results for (a) type 1: 10 × 50 µm^2 with 2 µm gap, (b) type 1: 30 × 30 µm^2 with 2 µm gap, (c) type 1: 40 × 40 µm^2 with 2 µm gap and (d) type 2: 30 × 30 µm^2 with 5 µm gap surface QW DILED structures.

The final structure at (d) emitted from both, left and right, side of the structure. Comparing this to the corresponding microscope images, where the emission originates from the bottom corners of the QW, the results are slightly different. Measuring other type 2 structures, all of them behaved differently. There were some

that emitted light only from the left side of the QW, some completely at the bottom of the QW, while others emitted throughout the whole QW. The reason for that all of the studied surface QW DILED structures behaved so differently is due to the quality of the InGaN QW. There are locations with different amount of indium in the QW creating these hotspots and differences to the emission of the surface QW DILEDs.

Figure 34 presents I-V curves for all surface QW DILED structures with different dimensions and structure types. In (a) is type 1 with 2 μm gaps, in (b) is type 1 with 5 μm gaps and in (c) is type 2 with 5 μm gaps. All the curves behaved quite diode-like, but are more abrupt when crossing threshold voltage, such as type 1: 40×40 μm^2 and 50×50 μm^2 with 5 μm gap in (b) with voltages above 70 V. Typically the threshold voltage was in the range of 40 V to 45 V, which are enormous compared to the similar values of the reference LED or even to buried DILED structures. A few structures activated with voltages below 6 V, namely type 1: 10×50 μm^2 and 50×50 μm^2 in (a). This would also indicate a significant parasitic parallel resistance of the structures in addition to a series resistance. Also, with other structures the series resistance is notable. The reason for the abrupt changes in the curves is due to the quality of the QW as well as the contact pads. Depositing high quality contacts on the p-GaN surface was challenging due to the etching damages.

Another possible reason for the high activating voltages could be due to weakly "activated" p-GaN. Mg atoms in the p-GaN are activated after the growth by removing some of it. After the activation, the p-GaN at the bottom might be passivated, because the growth is continued on top of it. Hydrogen is one those atoms that passivates the Mg atoms. When p-GaN is heated, some of the hydrogen atoms are removed, which in turn activates the Mg atoms. However, by continuing the growth, hydrogen is able to diffuse back into p-GaN which again passivates the Mg atoms, thus leaving p-GaN passivated. In order to obtain suitable quality for both doped p-GaN and contact pads, some appropriate engineering is required. Succeeding this the surface QW DILED could provide a potential solution, *e.g.*, for surface LEDs based on nanowires and surface plasmons.

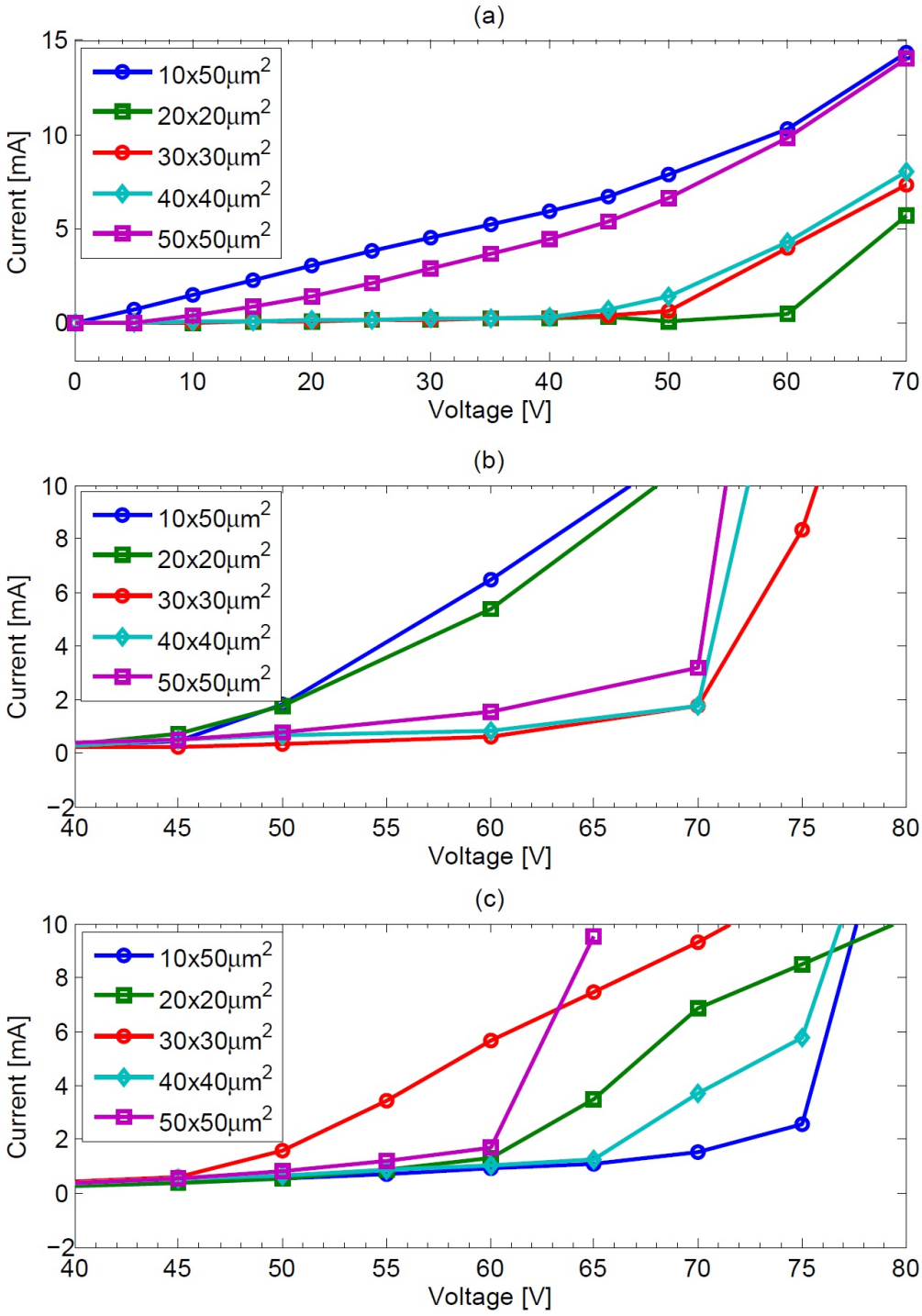

Figure 34: I-V curves for surface QW DILED structures for (a) type 1 with 2 μm gap, (b) type 1 with 5 μm gap and (c) type 2 with 5 μm gap.

5.5 Photoluminescence Results for All Structures

Figure 35 shows normalized PL results at room temperature for all studied structures, including the reference LED. Because all structures had some oscillating interference in the spectrum, especially the surface QW DILED and the Sample B DILED with peak wavelength at 480 nm, a smoothing spline was used with an appropriate parameter to get rid of the oscillation. The z-axis of the XYZ-measuring table was adjusted in each structure in order to obtain maximum intensity. In the case of Sample B DILED the height was set in order to obtain the maximum intensity for the first peak. The emission peaks occurred at 445 nm for Sample A, 391 nm, 428 nm and 480 nm for Sample B, 470 nm for surface QW DILED and 441 nm for reference LED (labeled as REF LED). The reference LED was not as much activated as was the buried DILED and surface QW DILED structures, but it showed the most clear band-to-band transition of GaN at 364 nm peak. This peak was not visible with Sample A nor surface QW DILED, except slightly in Sample B (not presented). However, it was clearly observed under the temperature controlled EL in the Sample B DILED in Figure 30. In all cases, no YL was observed under PL.

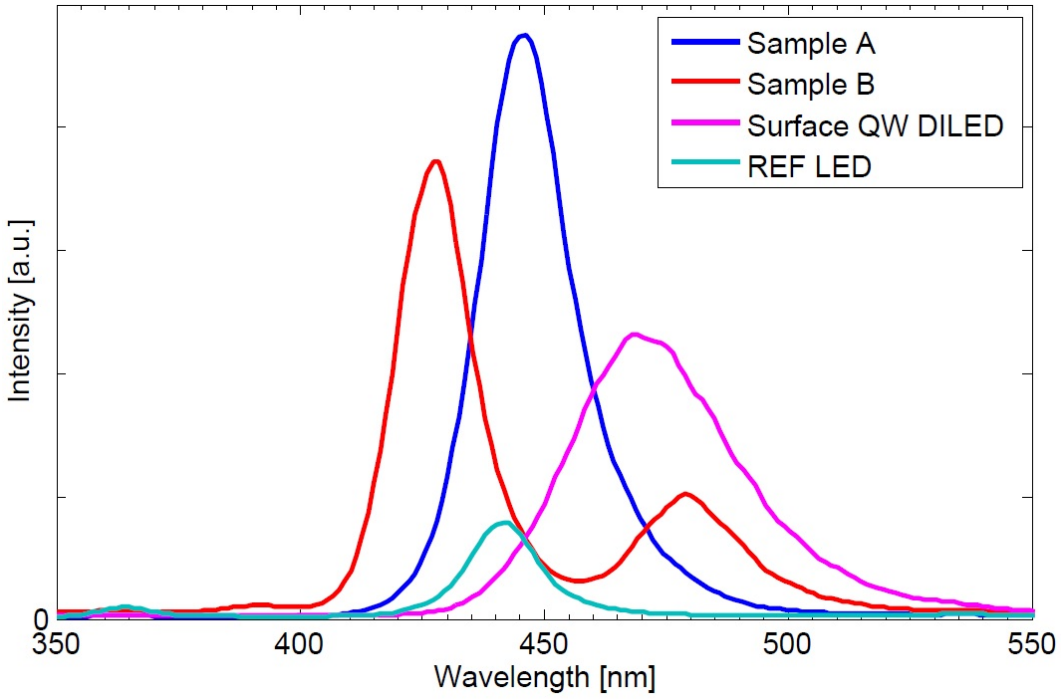

Figure 35: Normalized PL measurement for all studied devices at room temperature.

6 Conclusion

In this thesis, luminescence properties of novel GaN based diffusion injected LED, *i.e.*, DILED, structures were studied. The goal was to characterize and to determine the effectiveness of the DILED structures as new device design when implementing novel nanostructured LEDs, *e.g.*, based on nanowires or surface plasmons. The examined DILED structures represents a new LED design where the active region is located outside the p-n junction. Two different types of DILED structures were fabricated, a buried InGaN/GaN MQW DILED and a surface InGaN QW DILED. The buried MQW DILED had two slightly different types of samples, which were labeled as "Sample A" and "Sample B". The only difference between the samples was the number of QWs, indium compositions and the materials used in contact pads. Otherwise the structures were similar. In Sample A there were 5 QWs in the buried MQW stack, while in Sample B the number of QWs was 3 each with different indium composition. In both cases, there were comb-like fingers in the structure layout and the number of those fingers were either 1, 5, 10 or 20. Also, the widths of those fingers were either 2 μm, 5 μm, 10 μm, or 20 μm with lengths of 300 μm. In the case of surface QW DILED, there were two different types of structure layouts, which were referred as "type 1" and "type 2". The shape of the surface QW was either square or rectangle. The dimensions for the square QW varied from 20×20 μm^2 to 50×50 μm^2 either with 2 μm or 5 μm gap between the QW mesa and the n-contact. For the rectangle shaped QW the corresponding dimension was 10×50 μm^2 either with 2 μm or 5 μm gap. There was also a conventional LED fabricated in order to provide reference values in which the DILED structures were compared to.

The following measurements were carried out: EL, temperature controlled EL, PL and μ-PL. In both, Sample A and B, YL emission was observed under EL including temperature controlled EL measurements with low injection currents. However, the emission was much stronger in Sample A than was in Sample B. Also, YL was much stronger with wider finger widths. No YL was observed in surface QW DILED structures nor in Samples A and B under PL. Sample A emitted with peak wavelength of 445 nm with wide YL spectrum ranging from 500 nm up to 650 nm. Sample B emitted with peaks at 370 nm, 390 nm, 425 nm and 485 nm, which corresponds to band-to-band transition of GaN, the top, middle and bottom QWs, respectively. An interesting observation was obtained during temperature controlled EL. The emission of Sample A increased with elevated temperatures due to the increased diffusion current into the active region located outside the p-n junction. This is in contrast to the conventional LEDs. Also, Sample B indicated similar behavior mainly for the bottommost QW. The I-V curves of both samples showed typical diode-like behavior with threshold voltage of 3 V for Sample A and 4 V for Sample B. In the case of surface QW DILED, the corresponding voltages were mainly in the range of 40 V to 45 V. One possible reason for the high threshold voltages for surface QW DILED is due to the unoptimized contact pad quality. Another reason could be due to weakly activated p-GaN during growth. Both, Sample A and Sample B, showed relatively low EQE, optical output power and wall-plug efficiency. For Sample A

these values varied from 0.2 % to 0.5 % for EQE at 140 mA, 0.4 mW to 1 mW for output power and 0.06 % to 0.16 % for wall-plug efficiency. The corresponding values for Sample B ranged from 0.2 % to 0.5 %, 0.5 mW to 1.3 mW, and 0.11 % to 0.19 % for EQE, output power and wall-plug efficiency, respectively. However, the behavior of these figure of merit values was in contrast to those of conventional ones. Unlike conventional LEDs, with increasing injection current the value of EQE and output power increased in buried DILED structures. With proper device design and engineering, it is possible to improve the overall efficiency of GaN based LEDs.

The emission of surface QW DILED structures was observed with naked eye, but it was too weak to measure from either side (top or bottom) with optical fiber. In addition to I-V charasteristic, only PL and μ-PL measurements were carried out. However, microscope images during EL were taken, which indicated that type 1 surface QW DILED structures begins to emit from the n-side of the structure while type 2 emits from the p-side corners of the surface QW. The results from μ-PL shows great variety in emission locations due to the quality of InGaN QW during MOVPE growth. The indium concentration probably varies throughout the QW. In addition to the buried DILED structures, also the surface QW DILED structure provides an alternative current injection method and a new possibility for device design. DILED structures based on nanowires or surface plasmons may have potential to help overcome some of the challenges when developing GaN based LEDs. For future research, it would be desirable to fabricate these novel nanostructured DILED devices.

References

[1] Waide, P. & Tanishima, S. *Light's Labour's Lost: Policies for Energy-efficient Lighting*. Paris, OECD/IEA, 2006.

[2] Mottier, P. *LEDs for Lighting Applications*. Wiley, 2009. ISBN 978-184821-145-2.

[3] Nakamura, S. *The Roles of Structural Imperfections in InGaN based Blue Light-Emitting Diodes and Laser Diodes*. Science, vol. 281, no. 5379, pp. 956–961, 1998. DOI: 10.1126/science.281.5379.956.

[4] Hurni, C. A. *et al. Bulk GaN flip-chip violet light-emitting diodes with optimized efficiency for high-power operation*. Applied Physics Letters, vol. 106, p. 031101, 2015. DOI: 10.1063/1.4905873.

[5] Kivisaari, P. *From computational models to improved light-emitting diodes and new devices*. Aalto University publication series, Doctoral Dissertations, 198/2014. ISBN (printed) 978-952-60-5991-4. ISBN (pdf) 978-952-60-5992-1.

[6] Nguyen, H. P. T. *et al. p-Type Modulation Doped InGaN/GaN Dot-in-a-Wire White-Light-Emitting Diodes Monolithically Grown on Si(111)*. Nano letters, vol. 11, pp. 1919–1924, 2011. DOI: 10.1021/nl104536x.

[7] Homeyer, E. *et al. Enhanced light extraction from InGaN/GaN quantum wells with silver gratings*. Applied Physics Letters, vol. 102, p. 081110, 2013. DOI: 10.1063/1.4794066.

[8] Riuttanen, L. *et al. Diffusion injected multi-quantum well light-emitting diode structure*. Applied Physics Letters, vol. 104, no. 81102, 2014. DOI: 10.1063/1.4866343.

[9] Young, H. D. and Freedman, R. A. *Sears and Zemansky's university physics: with modern physics*. 11th ed. San Francisco, CA: Pearson, Addison Wesley, 2004. ISBN 0-8053-9185-1.

[10] Wikipedia, Wurtzite crystal structure, Wurtzite unit cell. http://en.wikipedia.org/wiki/Wurtzite_crystal_structure#/media/File:Wurtzite-unit-cell-3D-balls.png, May 2005.

[11] Sze, S. M. & Kwok, K. NG. *Physics of semiconductor devices*. 3rd ed. Wiley, 2007. ISBN 978-0-471-14323-9.

[12] Singh, J. *Semiconductor Optoelectronics: Physics and Technology*. New York: MacGraw-Hill, 1995. ISBN 0-07-057637-8.

[13] Ibach, H. & Lüth, H. *Solid-state physics: an introduction to principles of materials science*. 4th ed. New York: Springer, 2009. ISBN 978-3-540-93803-3.

[14] Sze, S. M. *Semiconductor devices: physics and technology.* 2nd ed. New York: Wiley, 2002. ISBN 0-471-33372-7.

[15] Harris, R. *Modern physics.* 2nd ed. San Francisco, CA: Pearson Addison-Wesley, 2008. ISBN 978-0-321-52667-0.

[16] Ju, Z. G. *et al. On the origin of the redshift in the emission wavelength of InGaN/GaN blue light emitting diodes grown with a higher temperature interlayer.* Applied Physics Letters, vol. 100, no. 12, p. 123503, 2012. DOI: 10.1063/1.3694054.

[17] Masui, H. *et al. Quantum-confined Stark effect on photoluminescence and electroluminescence characteristics of InGaN based light-emitting diodes.* Journal of Physics D: Applied Physics, vol. 41, no. 16, p. 165105, 2008. DOI: 10.1088/0022-3727/41/16/165105.

[18] Schubert, E. F. *Light-Emitting Diodes.* 2nd ed. Cambridge, U.K.: Cambridge University Press, 2006. ISBN 978-0-521-86538-8.

[19] Liu, Z. *et al. Effect of indium tin oxide (ITO) current spreading layer on the current uniformity of vertical structure GaN-based light-emitting diodes.* SPIE Proceedings, vol. 6841, 2008. DOI: 10.1117/12.760221.

[20] Nakamura, S. Mukai, T. and Senoh, M. *High-Power GaN P-N Junction Blue-Light-Emitting Diodes.* Japanese Journal of Applied Physics, vol. 30, no. 12A, pp. L1998–L2001, 1991. DOI: 10.1143/JJAP.30.L1998.

[21] Nakamura, S. Stephen, P. and Gerhard, F. *The blue laser diode: the complete story.* Berlin: Springer, 2000. ISBN 3-540-66505-6.

[22] Vurgaftman, I. and Meyer, J. R. *Band parameters for nitrogen-containing semiconductors.* Journal of Applied Physics, vol. 94, no. 6, p. 3675, 2003. DOI: 10.1063/1.1600519.

[23] Wu, J. *et al. Unusual properties of the fundamental band gap of InN.* Applied Physics Letters, vol. 80, no. 21, p. 3967, 2002. DOI: 10.1063/1.1482786.

[24] Walukiewicz, W. *et al. Optical properties and electronic structure of InN and In-rich group III-nitride alloys.* Journal of Crystal Growth, vol. 269, no. 1, pp. 119–127, 2004. DOI: 10.1016/j.jcrysgro.2004.05.041.

[25] Gibart, P. *Metal organic vapor phase epitaxy of GaN and lateral overgrowth.* Reports on Progress in Physics, vol. 67, no. 5, pp. 667–715, 2004. DOI: 10.1088/0034-4885/67/5/R02.

[26] Amano, H. *et al. Metalorganic vapor phase epitaxial growth of a high quality GaN film using an AlN buffer layer.* Applied Physics Letters, vol. 48, no. 5, p. 353, 1986. DOI: 10.1063/1.96549.

[27] Nakamura, S. *GaN growth using GaN buffer layer.* Japanese Journal of Applied Physics, vol. 30, no. 10A, pp. L1705–L1707, 1991. DOI: 10.1143/JJAP.30.L1705.

[28] Nakamura, S. and Mukai, T. *High-quality InGaN films grown on GaN films.* Japanese Journal of Applied Physics, vol. 31, no. 10B, pp. L1457–L1459, 1992. DOI: 10.1143/JJAP.31.L1457.

[29] Nakamura, S. *et al. Thermal annealing effects on p-type Mg-doped GaN films.* Japanese Journal of Applied Physics, vol. 31, no. 2B, pp. L139–L142, 1992. DOI: 10.1143/JJAP.31.L139.

[30] Piprek, J. *Efficiency droop in nitride-based light-emitting diodes.* Physica Status Solidi A, vol. 207, no. 10, pp. 2217–2225, 2010. DOI 10.1002/pssa.201026149.

[31] Piprek, J. *III-Nitride LED Efficiency Droop Models: A Critical Status Review.* Proc. NUSOD-13, pp. 107–108, 2013.

[32] Meyaard, D. S. *et al. Identifying the cause of the efficiency droop in GaInN light-emitting diodes by correlating the onset of high injection with the onset of the efficiency droop.* Applied Physics Letter, vol. 102, no. 25, p. 251114, 2013. DOI: 10.1063/1.4811558.

[33] Piprek, J. *LED droop: a critical review and novel solution.* Compound Semiconductor, vol. 20, pp. 44–48, 2014 (invited review). Cited February 20th, 2015. www.nusod.org/piprek/piprek14cs.pdf.

[34] Coleman, J. J. *Metalorganic chemical vapor deposition for optoelectronic devices.* Proceedings of the IEEE, vol. 85, no. 11, pp. 1715–1729, 1997. DOI: 10.1109/5.649647.

[35] Suihkonen, S. *Fabrication of InGaN quantum wells for LED applications.* TKK Dissertations 113. Espoo: Teknillinen korkeakoulu, 2008. ISBN (printed) 978-951-22-9268-8. ISBN (pdf) 978-951-22-9287-5.

[36] Garcia, I. *et al. MOVPE Technology for the Growth of III-V Semiconductor Structures.* 2007 Spanish Conference on Electron Devices, pp. 17–20, 2007. DOI: 10.1109/SCED.2007.383986.

[37] Riuttanen, L. *et al. Diffusion injection in a buried multi-quantum well light-emitting diode structure.* IEEE Transactions on Electron Devices, vol. 62, no. 3, pp. 902–908, 2015. DOI: 10.1109/TED.2015.2391117.

[38] Chichibu, S. *et al. Spontaneous emission of localized excitons in InGaN single and multiquantum well structures.* Applied Physics Letters, vol. 69, no. 27, p. 4188, 1996. DOI: 10.1063/1.116981.

[39] Mukai, T. Yamada, M. and Nakamura, S. *Current and Temperature Dependences of Electroluminescence of InGaN based UV/Blue/Green Light-Emitting Diodes.* Japanese Journal of Applied Physics, vol. 37, no. 11B, pp. L1358–L1361, 1998. DOI: 10.1143/JJAP.37.L1358.

[40] Wen-Yu, C. *et al. Effects of a prestrained InGaN interlayer on the emission properties of InGaN/GaN multiple quantum wells in a laser diode structure.* Chinese Physics B, vol. 22, no. 7, p. 076803, 2013. DOI: 10.1088/1674-1056/22/7/076803.

[41] Su, Y. K. Chi, G. C. and Sheu, J. K. *Optical properties in InGaN/GaN multiple quantum wells and blue LEDs.* Optical Materials, vol. 14, no. 3, pp. 205–209, 2000. DOI: 10.1016/S0925-3467(99)00138-X.

[42] Neugebauer, J. and Van de Walle, C. G. *Gallium vacancies and the yellow luminescence in GaN.* Applied Physics Letters, vol. 69, no. 4, p. 503, 1996. DOI: 10.1063/1.117767.

[43] Xu, F. J. *et al. Different origins of the yellow luminescence in as-grown high-resistance GaN and unintentional-doped GaN films.* Journal of Applied Physics, vol. 107, no. 2, p. 023528, 2010. DOI: 10.1063/1.3294965.

[44] Reshchikov, M. A. and Morkoc, H. *Luminescence properties of defects in GaN.* Journal of Applied Physics, vol. 97, no. 6, p. 061301, 2005. DOI: 10.1063/1.1868059.

[45] Lyons, J. L. Janotti, A. and Van de Walle, C. G. *Carbon impurities and the yellow luminescence in GaN.* Applied Physics Letters, vol. 97, no. 15, p. 152108, 2010. DOI: 10.1063/1.3492841.

[46] Huh, C. *et al. Temperature Dependence of Performance of InGaN/GaN MQW LEDs With Different Indium Compositions.* IEEE Electron Device Letters, vol. 25, no. 2, pp. 61–63, 2004, DOI 10.1109/LED.2003.822659.

[47] Heikkilä, O. Oksanen, J. and Tulkki, J. *The challenge of unity wall plug efficiency: The effects of internal heating on the efficiency of light emitting diodes.* Journal of Applied Physics, vol. 107, no. 3, p. 033105, 2010. DOI 10.1063/1.3285431.

[48] Kim, M. *et al. Origin of efficiency droop in GaN-basesd light-emitting diodes.* Applied Physics Letters, vol. 91, no. 18, p. 183507, 2007. DOI: 10.1063/1.2800290.

[49] Gong, Z. *et al. Size-dependent light output, spectral shift, and self-heating of 400 nm InGaN light-emitting diodes.* Journal of Applied Physics, vol. 107, no. 1, p. 013103, 2010. DOI: 10.1063/1.3276156.